Wideband Full-Duplex Phased Array with Joint Transmit and Receive Beamforming: Optimization and Rate Gains

Tingjun Chen, Mahmood Baraani Dastjerdi, Harish Krishnaswamy, and Gil Zussman

***Abstract*—Full-duplex (FD) wireless and phased arrays are both promising techniques that can significantly improve data rates in future wireless networks. However, integrating FD with transmit (Tx) and receive (Rx) phased arrays is extremely challenging, due to the large number of self-interference (SI) channels. Previous work relies on either RF canceller hardware or on analog/digital Tx beamforming (TxBF) to achieve SI cancellation (SIC). However, Rx beamforming (RxBF) and the data rate gain introduced by FD nodes employing beamforming have not been considered yet. We study FD phased arrays with joint TxBF and RxBF with the objective of achieving improved FD data rates. The key idea is to carefully select the TxBF and RxBF weights to achieve wideband RF SIC in the spatial domain with minimal TxBF and RxBF gain losses. Essentially, TxBF and RxBF are *repurposed*, thereby not requiring specialized RF canceller circuitry. We formulate the corresponding optimization problem and develop an iterative algorithm to obtain an approximate solution with provable performance guarantees. Using SI channel measurements and datasets, we extensively evaluate the performance of the proposed approach in different use cases under various network settings. The results show that an FD phased array with 9/36/72 elements can cancel the total SI power to below the noise floor with sum TxBF and RxBF gain losses of 10.6/7.2/6.9 dB, even at Tx power level of 30 dBm. Moreover, the corresponding FD rate gains are at least 1.33/1.66/1.68×.**

***Index Terms*—Full-duplex wireless; Phased array; Beamforming; Wideband self-interference cancellation; Optimization**

I. Introduction

Full-duplex (FD) wireless – simultaneous transmission and reception on the same frequency – has the potential to double the throughput and reduce latency, thereby has attracted significant attention [2], [3]. The fundamental challenge associated with FD wireless is the vast amount of self-interference (SI) leaking from the transmitter (Tx) into the receiver (Rx), which needs to be canceled to successfully recover the desired signal. Recent work has demonstrated practical levels of SI cancellation (SIC) at the antenna interface, RF/analog, and digital baseband [4]–[8].

Another important technology is Tx (resp. Rx) phased arrays which can substantially enhance the communication range through analog Tx beamforming (TxBF) (resp. Rx beamforming (RxBF)), a technique for directional signal transmission (resp. reception) utilizing spatial selectivity [9], [10]. TxBF/RxBF can provide significantly increased Tx/Rx signal power at the same link distance, or enhanced link distance at the same signal-to-noise ratio (SNR).

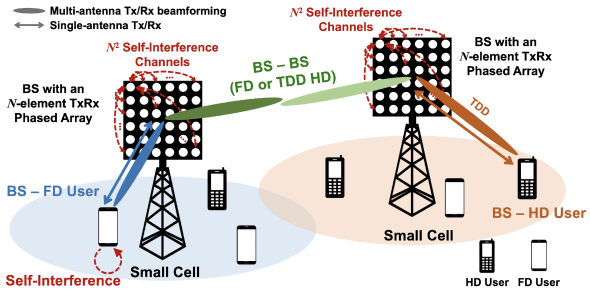

Fig. 1: Example network scenarios where a base station (BS) is equipped with an N-element TxRx phased array, employing Tx and Rx beamforming. Considered use cases: (i) *BS-User*: uplink-downlink (UL-DL) transmission between the BS and a user in HD (orange) or FD (blue) mode, and (ii) *BS-BS*: bidirectional transmission between two BSs in HD (beamforming in dark/light green in alternate time slots) or FD (simultaneous beamforming in dark/light green) mode.

Although combining FD with phased arrays can provide significantly improved data rates, it poses numerous challenges. First, in an N-element FD phased array (see Fig. 1), N^2 *SI channels between every pair of Tx and Rx elements need to be canceled in the RF domain*. Techniques using circuits (e.g., [11]) or alternating antenna placements (e.g., [12]) to achieve wideband RF SIC do not directly apply to an FD phased array. This is due to the fact that RF cancellers are expensive while the cancellation via antenna placements usually requires at least twice as many antennas. Accordingly, both techniques cannot scale to large phased arrays. gain of N [10], the total SI power can also potentially add up constructively by a factor of N^2. Therefore, innovative solutions are needed to achieve FD operation in phased arrays.

In this paper, we show that *by carefully selecting the Tx and Rx analog beamforming weights (a.k.a., beamformers), an FD phased array can simultaneously achieve wideband RF SIC with minimal TxBF and RxBF gain losses, and improved FD rate gains*. In other words, TxBF and RxBF can be *repurposed* to support wideband RF SIC with minimal performance degradation and without using any specialized canceller hardware. A key insight of our approach is that in multi-antenna systems, the *spatial* domain (i.e., across Tx and Rx elements) represents another dimension in which RF SIC can be achieved. The advantage of this approach is manifold: the RF SIC based on joint TxBF and RxBF (i) is *wideband* since the SI channels between every pair of Tx and Rx elements experience similar

This work was supported in part by NSF grants ECCS-1547406, CNS-1650685, CNS-1827923, and CNS-1910757, and the DARPA ACT and SPAR programs. A partial and preliminary version of this paper appeared in ACM MobiHoc'19 [1].

T. Chen is with the Department of Electrical and Computer Engineering, Duke University, Durham, NC 27708, USA. He was with the Department of Electrical Engineering, Columbia University, New York, NY 10027, USA (email: tingjun.chen@duke.edu).

M. Baraani Dastjerdi is with MixComm Inc. He was with the Department of Electrical Engineering, Columbia University, New York, NY 10027, USA (email: b.mahmood@columbia.edu).

H. Krishnaswamy and G. Zussman are with the Department of Electrical Engineering, Columbia University, New York, NY 10027, USA (e-mail: {harish, gil}@ee.columbia.edu).

delays, (ii) *does not* require specialized RF SIC circuitry or hardware, thus reducing the system complexity and total power consumption, (iii) is achieved before the digital domain, which largely reduces the analog-to-digital converter (ADC) dynamic range and power consumption, and (iv) will benefit from large-scale antenna arrays where a large number of TxBF and RxBF weights can be modified.

We consider network scenarios as depicted in Fig. 1, where a BS is an N-element, single-stream, FD phased array (see Fig. 3(a)). We consider two use cases where an FD BS communicates with: (i) a single-antenna user which is HD- or FD-capable (the *BS-User* case), or (ii) with another FD BS (the *BS-BS* case), and derive the data rate gain resulting from using FD. Specifically, the FD link objective is to *maximize the FD data rate gains* by optimizing the FD Tx and Rx beamformers with minimal TxBF and RxBF gain losses. We demonstrate the FD rate gains introduced by FD phased arrays employing TxBF and RxBF in various network settings. Based on the Argos FD channel measurements [13], [14], we show that in the BS-User case, a 36-element FD phased array with Tx power of 20 dBm can achieve maximum FD rate gains of 1.27/1.60/1.72$\times$ with 0/15/30 dB link SNR values, and with TxBF and RxBF gain losses of only 3.1 dB.

Based on the FD link objective, we formulate an optimization problem to jointly determine the optimal FD Tx and Rx beamformers. Due to its non-convexity and analytical intractability, we present a relaxed optimization problem and show that it achieves high accuracy. We then present two alternative convex optimization problems by leveraging the structural properties of the SI channel matrix and its coupling with the Tx and Rx beamformers. We develop an iterative algorithm that efficiently solves the alternative optimization problems with provable performance guarantees.

We numerically evaluate the network performance and the corresponding FD rate gains when using the iterative algorithm, based on SI channel measurements and datasets. Extensive evaluations are conducted under different network scenarios and a wide range of number of antennas, antenna array geometries, and Tx power levels. Specifically, the results show that an FD phased array with 9/36/72 elements can cancel the total SI power to below the noise floor with sum TxBF and RxBF gain losses of 10.6/7.2/6.9 dB, even at Tx power level of 30 dBm (note that the conventional HD TxBF and RxBF can provide sum TxBF and RxBF gains of 19.1/30.1/37.1 dB). Moreover, the *FD rate gains* in the BS-User case are at least 1.33/1.66/1.68$\times$ with $N = 9/36/72$. The FD rate gains in the BS-BS case are at least 1.53$\times$ with $N \geq 36$ in all considered SNR regimes. We also demonstrate the efficiency of the developed iterative algorithm.

To summarize, the main contributions of this paper are: (i) an FD phased array model that employs joint TxBF and RxBF for simultaneously achieving wideband RF SIC and high FD rate gains, (ii) an efficient iterative algorithm for obtaining the FD Tx and Rx beamformers with provable performance guarantees, and (iii) extensive evaluation of the proposed approach using realistic SI channel measurements and datasets.

The rest of the paper is organized as follows. We discuss related work in Section II, and provide background on phased arrays in Section III. In Section IV, we present the FD phased array model and FD link objective, followed by motivating examples in Section V. In Section VI, we present the optimization problems and the iterative algorithm. We evaluate the performance via measurement-based simulations in Section VII and conclude in Section VIII.

II. Related Work

Recent work focused on the design and implementation of FD radios and systems, either using off-the-shelf components [4], [5], [15] or based on integrated circuits (ICs) [3], [7], [8] (see the review in [2] and references therein). For single-antenna FD, a pair of Tx and Rx antennas with proper separation, or a shared antenna interface using a circulator, have been used. Moreover, a single-antenna open-access FD radio design has been integrated in the ORBIT wireless testbed [16] to allow the community to experiment with FD wireless. In this case, RF SIC is achieved by an *additional* cancellation circuitry. FD MIMO radio implementations have been presented in [11], [12], where up to 3 Tx/Rx antennas are considered and RF SIC is achieved using either RF cancellers or through alternating antenna placements.

At the higher layers, FD rate gain with single-antenna FD radios has been studied analytically at the link-level [17], and experimentally at the link- and network-level [8]. Moreover, recent work explores medium access control and scheduling in FD networks [18]–[22] as well as FD relays [23]–[26]. FD also facilitates different applications including improved PHY layer security [27], neighbor discovery [28], and localization [29].

Most relevant to our work are [23], [24], [30]–[32]. In particular, [30] considers an FD multi-user MIMO downlink channel with *separate* Tx and Rx antennas and applies *only digital* TxBF to achieve RF SIC. JointNull is proposed in [31] as an SIC architecture with a varying number of analog cancellers, where the antenna configuration and transmit precoder are optimized to achieve maximized FD rates. This differs from our approach, which is based on joint analog TxBF and RxBF and results in lower power consumption. RF SIC in the spatial domain has also been considered for FD MIMO relays [23], [24]. On the other hand, in [32], *narrowband* RF SIC is achieved via *only* analog TxBF for small-scale (i.e., 8 elements) phased arrays with separate Tx and Rx antennas. Our previous work [33] focuses on IC implementations of an 8-element FD phased array. However, the optimization of the TxBF and RxBF for an FD phased array with varying numbers of antennas and geometries, and the corresponding FD rate gains in different network scenarios have not be addressed.

To the best of our knowledge, this is *the first fundamental study of an FD phased array employing joint TxBF and RxBF to achieve wideband RF SIC and FD rate gains*. We believe that the proposed approach is beneficial to other problems related to multi-antenna systems applying different beamforming techniques (e.g., hybrid analog/digital beamforming [34]) at different frequencies (e.g., millimeter-wave bands [35]).

III. Background on Phased Arrays

In this section, we follow [10] and provide background on phased arrays and beamforming in the half-duplex setting.

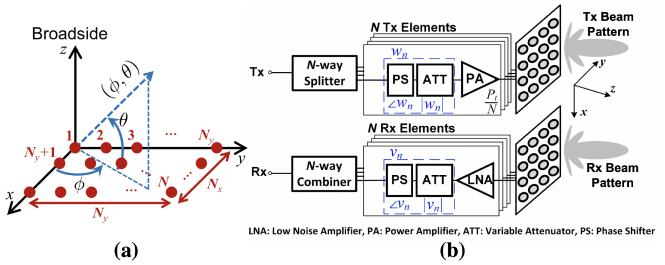

Fig. 2: (a) An example N-element rectangular antenna array in a spherical coordinate system, (b) block diagrams of N-element Tx (top) and Rx (bottom) phased arrays in the HD setting.

Beamforming is a technique that uses an antenna phased array to achieve directional signal transmission or reception. For completeness, we describe Tx and Rx phased arrays, and Tx and Rx beamforming (TxBF and RxBF). We provide an overview of the steering vector and Tx/Rx arrays, followed by the important characteristics of beamforming including array factor, beam pattern, and beamforming gain.

Steering Vector. Denote by N the number of antennas in the array (see Fig. 2(a)). A spherical coordinate system is considered where the azimuth and elevation angles are denoted by ϕ and θ, respectively. Let $s_n(\phi,\theta)$ be the relevant phase delay experienced by a plane wave as it departs/reaches the n^{th} Tx/Rx element in the spatial direction of (ϕ,θ). Consider an example N-element rectangular antenna array with N_x rows and N_y columns ($N_x \cdot N_y = N$), where the antennas are indexed as shown in Fig. 2(a). Assuming half-wavelength spacing between adjacent antennas, $s_n(\phi,\theta)$ for the n^{th} element at location (n_x, n_y), where $n = (n_x-1)N_y + n_y$, is

$$s_n(\phi,\theta) = e^{j\pi[(n_x-1)\cos\theta\cos\phi+(n_y-1)\cos\theta\sin\phi]},\ \forall n_x, n_y.$$

The *steering vector* in the direction of (ϕ,θ) is then given by $\mathbf{s}(\phi,\theta) = [s_n(\phi,\theta)] \in \mathbb{C}^N$, which depends on the antenna array geometry.

Transmit (Tx) and Receive (Rx) Arrays, and Analog Beamformer. As illustrated in Fig. 2(b), in an N-element single-stream Tx array with total Tx power of P_{t}, each Tx element consists of a fixed gain power amplifier (PA), a variable gain attenuator (ATT), and a voltage variable phase shifter (PS) that can be controlled by a digital-to-analog converter. We assume that the Tx array has a total maximum Tx power of P_{t} after the PAs. Symmetrically, in an N-element single-stream Rx array, each Rx element consists of a fixed gain low noise amplifier (LNA), a variable gain attenuator, and a voltage variable phase shifter.Denote by P_{nf} the noise floor of a single Rx element. Then, the Rx array has an array noise floor of $N \cdot P_{\text{nf}}$ due to the aggregated noise from all Rx elements. We assume the followings: (i) with an ideal power splitter and identical PAs, each Tx element has a maximum Tx power of P_{t}/N, and (ii) the LNA of each Rx element has a unit gain of 1.

An *analog beamformer* is the set of complex-valued weights applied to each element *relative* to that of the first element. Specifically, denote the weight applied to the n^{th} Tx (resp. Rx) element by $w_n = |w_n| \cdot e^{j\angle w_n}$ (resp. $v_n = |v_n| \cdot e^{j\angle v_n}$) with amplitude $|w_n|$ (resp. $|v_n|$) and phase $\angle w_n$ (resp. $\angle v_n$). In particular, $|w_n|^2, |v_n|^2 \le 1$ represent the variable gain on the n^{th} Tx/Rx element controlled by the attenuator. $\angle w_n, \angle v_n \in [-\pi,\pi]$ represent the phase on the n^{th} Tx/Rx element controlled by the phase shifter. The vectors $\mathbf{w} = [w_n] \in \mathbb{C}^N$ and $\mathbf{v} = [v_n] \in \mathbb{C}^N$ are called the *Tx and Rx (analog) beamformers*, respectively.

Array Factor, Beam Pattern, and Beamforming Gain. An analog beamformer features $(N-1)$ complex-valued degrees of freedom (DoF), which are the reconfigurable parameters in an N-element phased array. These DoF are typically configured to alter the *beam pattern* (see Fig. 2(b)) to enhance the signal directivity and/or to suppress interference by constructing nulls. The far-field Tx and Rx *array factors* in the direction of (ϕ,θ), which quantify the effect of combining weighted transmitting Tx and receiving Rx elements, are given by [10]

$$\begin{cases} A_{\text{t}}(\phi,\theta) = \sum_{n=1}^{N}(s_n(\phi,\theta)\cdot w_n) = \mathbf{s}^\top(\phi,\theta)\cdot\mathbf{w} \in \mathbb{C}, \\ A_{\text{r}}(\phi,\theta) = \sum_{n=1}^{N}(s_n(\phi,\theta)\cdot v_n) = \mathbf{s}^\top(\phi,\theta)\cdot\mathbf{v} \in \mathbb{C}. \end{cases}$$

The far-field Tx and Rx *beam patterns* are defined as

$$\begin{cases} E_{\text{t}}(\phi,\theta) = |A_{\text{t}}(\phi,\theta)|^2 = |\mathbf{s}^\top(\phi,\theta)\cdot\mathbf{w}|^2, \\ E_{\text{r}}(\phi,\theta) = |A_{\text{r}}(\phi,\theta)|^2 = |\mathbf{s}^\top(\phi,\theta)\cdot\mathbf{v}|^2. \end{cases} \quad (1)$$

The *Tx beamforming (TxBF) gain* (resp. *Rx beamforming (RxBF) gain*) is defined as the power gain of the Tx (resp. Rx) signal in the far-field normalized to the maximum total Tx (resp. Rx) power. Denote by $G_{\text{t}}(\phi,\theta)$ and $G_{\text{r}}(\phi,\theta)$) the TxBF gain and RxBF gain in the spatial direction of (ϕ,θ), respectively. They are given by

$$\begin{cases} G_{\text{t}}(\phi,\theta) = E_{\text{t}}(\phi,\theta)/N = |\mathbf{s}^\top(\phi,\theta)\cdot\mathbf{w}|^2/N, \\ G_{\text{r}}(\phi,\theta) = E_{\text{r}}(\phi,\theta)/N = |\mathbf{s}^\top(\phi,\theta)\cdot\mathbf{v}|^2/N. \end{cases} \quad (2)$$

Denote the *desired* Tx and Rx beam-pointing directions by $(\phi_{\text{t}},\theta_{\text{t}})$ and $(\phi_{\text{r}},\theta_{\text{r}})$. Let $\mathbf{s}_{\text{t}}$ and $\mathbf{s}_{\text{r}}$ be the steering vectors in the desired Tx and Rx beam-pointing directions, given by

$$\mathbf{s}_{\text{t}} = \mathbf{s}(\phi_{\text{t}},\theta_{\text{t}}),\ \mathbf{s}_{\text{r}} = \mathbf{s}(\phi_{\text{r}},\theta_{\text{r}}).$$

Then, the (complex-valued) Tx and Rx array factors in the desired beam-pointing directions, denoted by a_{t} and a_{r}, are then given by

$$a_{\text{t}} = A_{\text{t}}(\phi_{\text{t}},\theta_{\text{t}}) = \mathbf{s}_{\text{t}}^\top\mathbf{w},\ a_{\text{r}} = A_{\text{r}}(\phi_{\text{r}},\theta_{\text{r}}) = \mathbf{s}_{\text{r}}^\top\mathbf{v}. \quad (3)$$

Therefore, the TxBF and RxBF gains in $(\phi_{\text{t}},\theta_{\text{t}})$ and $(\phi_{\text{r}},\theta_{\text{r}})$, denoted by g_{t} and g_{r}, are given by

$$g_{\text{t}} = |a_{\text{t}}|^2/N,\ g_{\text{r}} = |a_{\text{r}}|^2/N. \quad (4)$$

Note that since g_{t} and g_{r} are the normalized power gains introduced by TxBF and RxBF, respectively, they *do not* depend on the absolute power levels of the Tx and Rx signals.

Conventional (Half-Duplex) TxBF and RxBF. It is known that by setting $\mathbf{w} = \mathbf{s}_{\text{t}}^*$ (resp. $\mathbf{v} = \mathbf{s}_{\text{r}}^*$), a maximum Tx (resp. Rx) array factor of N and a maximum TxBF (resp. RxBF) gain of N in the desired beam-pointing direction can be achieved [10], i.e.,

$$a_{\text{t}}^{\max} = \mathbf{s}_{\text{t}}^\top\mathbf{s}_{\text{t}}^* = N,\ a_{\text{r}}^{\max} = \mathbf{s}_{\text{r}}^\top\mathbf{s}_{\text{r}}^* = N,\ g_{\text{t}}^{\max} = g_{\text{r}}^{\max} = N. \quad (5)$$

We refer to $\mathbf{w}_{\text{conv}} = \mathbf{s}_{\text{t}}^*$ (resp. $\mathbf{v}_{\text{conv}} = \mathbf{s}_{\text{r}}^*$) as the *conventional HD Tx (resp. Rx) beamformers*.

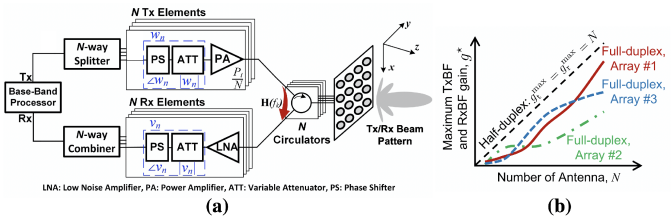

(a) (b)

Fig. 3: (a) Block diagram of an N-element FD phased array with SI channel matrix, $\mathbf{H}(f_k)$, where a Tx and an Rx phased arrays are connected to the antennas through circulators, (b) illustration of the relationship between the maximum TxBF and RxBF gains, $g_{\mathrm{t}}^\star = g_{\mathrm{r}}^\star = g^\star$, that can be achieved by an FD phased array after repurposing TxBF and RxBF for wideband RF SIC, and the number of antennas, N, for various array geometries.

IV. Model, Rates, and Objective

In this section, we present the model of an FD phased array node combining TxBF and RxBF, as well as the corresponding FD TxBF and RxBF gains. Then, we discuss the data rate gains obtained by FD and the FD link objective.

A. FD Phased Array Model

We consider an FD phased array node as depicted in Fig. 3(a). A BS is equipped with an N-element *FD phased array* with N unit-gain antennas, N circulators, and N Tx/Rx elements, where TxBF and RxBF are applied. Each antenna is *shared* between a pair of Tx and Rx elements via a circulator. For HD operation, the phased array will activate only N Tx or Rx elements. As shown in Fig. 1, a user has *a single antenna* and does not apply beamforming. We use b and u in the subscript to denote the BS and user. We consider a wireless bandwidth of B that is divided into K orthogonal frequency channels indexed by $k \in \{1, \ldots, K\}$, where f_k is the center frequency of the k^{th} channel. One example is OFDM-based system with K subcarriers over bandwidth of B.

SI Channel Matrix. Similar to [30], we let $H_{nn}(f_k), \forall n$, denote the frequency response of the SI channel from the n^{th} Tx element to the n^{th} Rx element at frequency $f_k, \forall k$, and let $H_{mn}(f_k), \forall m \neq n$, denote the frequency response of the cross-talk SI (CTSI) channel from the n^{th} Tx element to the m^{th} Rx element at frequency $f_k, \forall k$. We then denote $\mathbf{H}(f_k) = [H_{mn}(f_k)] \in \mathbb{C}^{N \times N}$ as the *SI channel matrix* of the TxRx array at frequency $f_k, \forall k$, consisting of all the N^2 SI and CTSI channels, as shown in Fig 1. We assume $|H_{mn}(f_k)| \leq 1, \forall i, j, k$, due to the propagation loss of the Tx signal. Ideally, due to channel reciprocity, $H_{mn}(f_k) = H_{nm}(f_k), \forall k$, for any Tx and Rx element pair (n, m), resulting in $\mathbf{H}(f_k) = \mathbf{H}^\top(f_k)$. However, as we will show in Section VII-A, this does not hold in a realistic environment, due to effects such as imperfections of antenna matching and environmental interference and noise.[1]

Use Cases. We consider four use cases as depicted in Fig. 1:

(i) *BS-User (HD or FD)*: uplink-downlink (UL-DL) transmission between a BS and a user in HD (orange) or FD (blue) mode,

(ii) *BS-BS (HD or FD)*: bidirectional transmission between two BSs in HD (beamforming in dark/light green in alternate time slots) or FD (simultaneous beamforming in dark/light green) mode.

The cases where the BSs or the user operate in HD mode and the channel is shared in a TDD manner are considered as the *benchmark HD cases*. When operating in FD mode, a BS applies simultaneous TxBF and RxBF when communicating with an FD user or another FD BS. We also assume that the BS has the information about the direction of another BS or an intended user (that can be spatially distributed in the network).

Self-Interference-to-Noise Ratio (XINR) under TxBF and RxBF. For an FD node, XINR is defined as the ratio between the residual SI power after SIC (across the RF/analog and digital domains) and the noise floor. Denote by $\gamma_{bb}(f_k)$ and $\gamma_{uu}(f_k)$ the XINR of the BS and the user at frequency (subcarrier) f_k, respectively, when operating in FD mode. Since our focus is on the SIC at the BS with TxBF and RxBF, we assume that a user can always cancel its SI to below the noise floor, i.e., $\gamma_{uu}(f_k) \leq 1, \forall k$ [7], [8]. Accordingly, a user transmits at the maximum possible power level when operating in either HD or FD mode.

For the BS, denote by $P_{\text{SI}}^{\text{bf}}(f_k)$ the SI power under TxBF and RxBF, and by SIC_{dig} the amount of achievable digital SIC.[2] The residual SI power after SIC is thus $P_{\text{SI}}^{\text{bf}}(f_k)/SIC_{\text{dig}}$. Recall that the BS has a noise floor of (NP_{nf}). Accordingly, the XINR at frequency (subcarrier) f_k is given by

$$\gamma_{bb}(f_k) = \frac{P_{\text{SI}}^{\text{bf}}(f_k)}{SIC_{\text{dig}} \cdot (NP_{\text{nf}})}, \ \forall k. \tag{6}$$

We now derive $\gamma_{bb}(f_k)$ under joint TxBF and RxBF. Without loss of generality, we assume a wideband (e.g., OFDM) transmit symbol $x(f_k) \in \mathbb{C}$ with unit power of $|x(f_k)|^2 = 1, \forall k$. The received SI symbol, denoted by $y(f_k) \in \mathbb{C}$, is given by

$$\begin{aligned} y(f_k) &= \textstyle\sum_{m=1}^{N} \sum_{n=1}^{N} \left[w_n H_{mn}(f_k) v_m\right] \cdot \sqrt{\frac{P_{\text{t}}}{N}} \cdot x(f_k) + z \\ &= \sqrt{\frac{P_{\text{t}}}{N}} \cdot \mathbf{v}^\top \mathbf{H}(f_k) \mathbf{w} \cdot x(f_k) + z, \ \forall k, \end{aligned}$$

where z is the additive white Gaussian noise. Then, the SI power is given by

$$P_{\text{SI}}^{\text{bf}}(f_k) = |y(f_k)|^2 = |\mathbf{v}^\top \mathbf{H}(f_k) \mathbf{w}|^2 \cdot \tfrac{P_{\text{t}}}{N}, \ \forall k. \tag{7}$$

Plugging (7) into (6) yields the XINR of the BS:

$$\gamma_{bb}(f_k) = \frac{|y(f_k)|^2}{SIC_{\text{dig}} \cdot (NP_{\text{nf}})} = \frac{|\mathbf{v}^\top \mathbf{H}(f_k) \mathbf{w}|^2}{SIC_{\text{dig}} N P_{\text{nf}}} \cdot \frac{P_{\text{t}}}{N}, \ \forall k. \tag{8}$$

B. FD Beamformers and Beamforming Gains

A maximum TxBF and RxBF gain of N can be achieved under the conventional HD Tx and Rx beamformers, $\mathbf{w}_{\text{conv}}$

[1] Note that our model and results also apply to an FD phased array where the Tx and Rx arrays are equipped with *seperate* antennas, which requires twice many antenna elements (as illustrated in Fig. 3(a)). Such separated Tx and Rx antennas usually provide better isolation (i.e., smaller values of $|H_{mn}(f_k)|$) than a shared antenna interface.

[2] We assume that SIC_{dig} is a positive constant across frequency. For example, [8] achieves 43 dB digital SIC (i.e., $SIC_{\text{dig}} = 10^{\frac{43}{10}}$) based on Volterra series and a least-square problem (more details can be found in [5]).

and $\mathbf{v}_{\text{conv}}$ (see (5)). However, as we will show in Section VII-C, the XINR under $\mathbf{w}_{\text{conv}}$ and $\mathbf{v}_{\text{conv}}$ is significant, i.e., $\gamma_{bb}(f_k) \gg 1, \forall k$. Therefore, using these beamforming weights is impractical for a BS operating in FD mode.

To support FD operation, we aim to achieve wideband RF SIC in an FD phased array *only* through manipulating the TxBF and RxBF weights, $\mathbf{w}$ and $\mathbf{v}$, thereby not requiring specific RF canceller hardware or circuitry (see Section I). Specifically, by properly selecting $\mathbf{w}$ and $\mathbf{v}$, we aim to achieve: (i) cancellation of SI to below the array noise floor (i.e., $\text{XINR}(f_k) = \gamma_{bb}(f_k) \leq 1, \forall k$), and (ii) maximum FD data rate gain. However, $\mathbf{w}$ and $\mathbf{v}$, termed as the *FD Tx and Rx beamformers*, may not achieve the maximum TxBF and RxBF gain of N as in the conventional HD setting. Accordingly, we define the optimal equal FD TxBF and RxBF gain as follows.

Proposition 4.1 (Optimal Equal FD TxBF and RxBF Gain)**.** *For a given FD phased array with $\mathbf{H}(f_k)$ and P_t, the optimal equal FD TxBF and RxBF gain is the equal maximum TxBF and RxBF gains, denoted by $g_t^\star = g_r^\star = g^\star$, that can be achieved while satisfying $\gamma_{bb}(f_k) \leq 1, \forall k$.*

To quantify the performance of FD TxBF and RxBF, we present the following definition.

Definition 4.1 (TxBF and RxBF Gain Losses)**.** *For a pair of Tx and Rx beamformers that respectively achieve FD TxBF and RxBF gains of g_t and g_r, while satisfying $\gamma_{bb}(f_k) \leq 1, \forall k$, the TxBF gain loss is defined as the ratio between the maximum HD TxBF gain and g_t, i.e., (N/g_t). Symmetrically, the RxBF gain loss is (N/g_r).*

The TxBF and RxBF gain losses are typically represented in dB. For example, a 3 dB TxBF gain loss means that the far-field Tx power is reduced by half, since $g_{\text{t}} = 0.5N \Rightarrow 10\log_{10}(N/g_{\text{t}}) = 3\,\text{dB}$. Similarly, a 6 dB TxBF gain loss corresponds to $g_{\text{t}} = 0.25N$.

Fig. 3(b) illustrates the relationship between $g^\star$ (given by Proposition 4.1) and the number of antennas, N, for various array geometries, where different antenna arrays may have different values of $g^\star$. In particular, for a given FD phased array with $\mathbf{H}(f_k)$ and Tx power level P_{t}, there exists a pair of optimal FD Tx and Rx beamformers that achieves $g^\star$ while satisfying $\gamma_{bb}(f_k) \leq 1, \forall k$. The FD phased array can achieve higher values of $g^\star$ with increased value of N, since a larger number of Tx and Rx weights can be adjusted.

C. Sum Link Rate and FD Rate Gain

We now derive the HD and FD data rates and the effect of the optimal FD TxBF and RxBF gain on the FD rates. Denote by γ the average link SNR without beamforming, i.e., using a single Tx element (with total Tx power, P_{t}) and a single Rx element (with noise floor, P_{nf}). We use Shannon's capacity formula to compute the rate on a link with bandwidth, B, and link SNR, γ. Since the TxBF and RxBF gains, g_{t} and g_{r}, are independent of the absolute power of the Tx and Rx signals (see Section III), the link SNR improvement introduced by beamforming equals to g_{t} and g_{r} in the desired Tx and Rx beam-pointing directions, respectively.

For the BS-User case, we denote by γ_{bu} ($u \to b$) and γ_{ub} ($b \to u$) the UL and DL SNRs, respectively. For the BS-BS case, we index the BSs by b_1 and b_2 and denote the link SNRs by $\gamma_{b_1 b_2}$ ($b_2 \to b_1$) and $\gamma_{b_2 b_1}$ ($b_1 \to b_2$). The sum of the HD link rates in both cases, when the BSs and user operate in HD mode and share the channel in a TDD manner equally (i.e., each link is activated for 50% of the time), are given by

$$r^{\text{HD}}_{\text{BS-User}} = \tfrac{B}{2}\big[\log_2\left(1 + N\gamma_{bu}\right) + \log_2\left(1 + N\gamma_{ub}\right)\big], \tag{9}$$

$$r^{\text{HD}}_{\text{BS-BS}} = \tfrac{B}{2}\big[\log_2\left(1 + N^2\gamma_{b_1 b_2}\right) + \log_2\left(1 + N^2\gamma_{b_2 b_1}\right)\big]. \tag{10}$$

In particular, the HD UL and DL SNR values in the BS-User case (9), $N\gamma_{bu}$ and $N\gamma_{ub}$, result from the maximum RxBF and TxBF gains of N in the desired beam-pointing directions. Similarly, the SNR improvements in the BS-BS case (10), which are factors of $g_{\text{t}}^{\max} g_{\text{r}}^{\max} = N^2$ for both $\gamma_{b_1 b_2}$ and $\gamma_{b_2 b_1}$, stem from the combined TxBF and RxBF gains of both BSs.

When the BSs and user operate in FD mode, the FD link SNRs are functions of the degraded TxBF and RxBF gains, $g_{\text{t}}^\star$ and $g_{\text{r}}^\star$, and the frequency-dependent XINR of the BS and user, $\gamma_{bb}(f_k)$ and $\gamma_{uu}(f_k)$, respectively. As a result, the sum of the FD link rates in both use cases are

$$r^{\text{FD}}_{\text{BS-User}} = \tfrac{B}{K}\sum_{k=1}^{K}\big[\log_2\left(1 + \tfrac{g_{\text{r}}^\star \gamma_{bu}}{1+\gamma_{bb}(f_k)}\right) + \log_2\left(1 + \tfrac{g_{\text{t}}^\star \gamma_{ub}}{1+\gamma_{uu}(f_k)}\right)\big], \tag{11}$$

$$r^{\text{FD}}_{\text{BS-BS}} = \tfrac{B}{K}\sum_{k=1}^{K}\big[\log_2\left(1 + \tfrac{g_{\text{t}}^\star g_{\text{r}}^\star \gamma_{b_1 b_2}}{1+\gamma_{bb}(f_k)}\right) + \log_2\left(1 + \tfrac{g_{\text{t}}^\star g_{\text{r}}^\star \gamma_{b_2 b_1}}{1+\gamma_{bb}(f_k)}\right)\big]. \tag{12}$$

Due to the coupling between $g_{\text{t}}^\star$, $g_{\text{r}}^\star$, and $\gamma_{bb}(f_k)$ through the Tx and Rx beamformers, $\mathbf{w}$ and $\mathbf{v}$ (see (8)), and the frequency-dependent $\mathbf{H}(f_k)$, maximizing (11)–(12) presents numerous challenges. To allow analytical tractability, we approximate the FD sum rates in (11)–(12) by setting $\gamma_{uu}(f_k) = \gamma_{bb}(f_k) = 1, \forall k$. We refer to the approximated FD sum rates as $\widetilde{r}^{\text{FD}}_{\text{BS-User}}$ and $\widetilde{r}^{\text{FD}}_{\text{BS-BS}}$, respectively, and they are given by

$$\widetilde{r}^{\text{FD}}_{\text{BS-User}} = B\big[\log_2\left(1 + \tfrac{g_{\text{r}}^\star \gamma_{bu}}{2}\right) + \log_2\left(1 + \tfrac{g_{\text{t}}^\star \gamma_{ub}}{2}\right)\big], \tag{13}$$

$$\widetilde{r}^{\text{FD}}_{\text{BS-BS}} = B\big[\log_2\left(1 + \tfrac{g_{\text{t}}^\star g_{\text{r}}^\star \gamma_{b_1 b_2}}{2}\right) + \log_2\left(1 + \tfrac{g_{\text{t}}^\star g_{\text{r}}^\star \gamma_{b_2 b_1}}{2}\right)\big]. \tag{14}$$

Since we aim to achieve $\gamma_{bb}(f_k) \leq 1$ (0 dB) for an FD phased array and recall that $\gamma_{uu}(f_k) \leq 1$, $\widetilde{r}^{\text{FD}}_{\text{BS-User}}$ and $\widetilde{r}^{\text{FD}}_{\text{BS-BS}}$ are *lower bounds* of the FD sum rates, $r^{\text{FD}}_{\text{BS-User}}$ and $r^{\text{FD}}_{\text{BS-BS}}$, in (11)–(12).

In the rest of the paper, we focus on maximizing $\widetilde{r}^{\text{FD}}_{\text{BS-User}}$ and $\widetilde{r}^{\text{FD}}_{\text{BS-BS}}$ under the optimal equal FD TxBF and RxBF gain given by Proposition 4.1. We define the *FD rate gain* in the BS-User case as the ratio between the FD sum rate lower bound (13) with $g_{\text{t}}^\star = g_{\text{r}}^\star = g^\star$ and the HD sum rate (9). Similarly, we define the FD rate gain in the BS-BS case as the ratio between the FD sum rate lower bound (14) with $g_{\text{t}}^\star = g_{\text{r}}^\star = g^\star$ and the HD sum rate (10).[3]

[3]While it would be beneficial to consider non-equal FD TxBF and RxBF gains co-optimized with the link SNR values, this is left for future work. Nevertheless, the case with optimal equal FD TxBF and RxBF gains (Proposition 4.1) still remains as a performance lower bound.

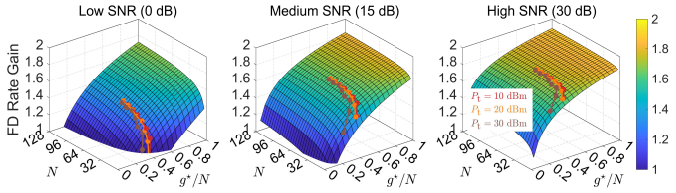

Fig. 4: FD rate gain in the BS-User case with varying number of antennas, N, and the normalized optimal equal FD TxBF and RxBF gain, $g^\star/N$, for different link SNR values $\gamma \in \{0, 15, 30\}$ dB. The relationships between $g^\star/N$ and N, based on the Argos traces [13], are also overlayed on the surface with $P_{\mathrm{t}} \in \{10, 20, 30\}$ dBm.

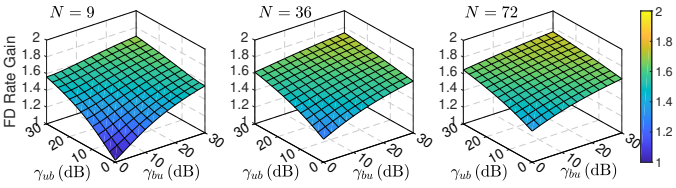

Fig. 5: FD rate gain in the BS-User case with varying UL and DL SNR values, γ_{bu} and γ_{ub}, respectively, with $N \in \{9, 36, 72\}$ and 3 dB TxBF and RxBF gain loss (i.e., $g^\star = N/2$).

D. FD Link Objective

Our objective is to maximize the FD rate gains in the two FD use cases. Based on the observation above, our goal is to obtain the optimal FD Tx and Rx beamformers, $\mathbf{w}$ and $\mathbf{v}$, that maximize TxBF and RxBF gains, g_{t} and g_{r}, while achieving sufficient amount of RF SIC, i.e.,

$$\gamma_{bb}(f_k) \le 1, \ \forall k, \\ \Leftrightarrow |\mathbf{v}^\top \mathbf{H}(f_k)\mathbf{w}|^2 \cdot \tfrac{P_{\mathrm{t}}}{N} \le SIC_{\mathrm{dig}} \cdot (NP_{\mathrm{nf}}) := N\beta, \ \forall k, \quad (15)$$

where $\beta := SIC_{\mathrm{dig}} P_{\mathrm{nf}}$ is a constant independent of N and P_{t}. Next, we first present the benefits introduced by FD phased arrays in terms of FD rate gains (Section V). Then, we present the corresponding problem formulation (Section VI).

V. Motivating Examples

In this section, we illustrate the FD rate gains obtained by FD phased arrays with joint TxBF and RxBF, where the FD rate gains are computed as described in Section IV-C. We provide motivating examples illustrating that higher values of the optimal equal FD TxBF and RxBF gain, $g_{\mathrm{t}}^\star = g_{\mathrm{r}}^\star = g^\star$ (see Definition 4.1), lead to increased FD rate gains. We will describe how to obtain $g^\star$ in Section VI-A (Opt-TxRx).

BS-User Case: We first consider equal UL and DL SNR values of $\gamma_{bu} = \gamma_{ub} = \gamma$ in low, medium, and high SNR regimes with $\gamma \in \{0, 15, 30\}$ dB.These values correspond to typical Rx signal levels in an LTE network, where the user is at the edge, middle, and center of the small cell. Fig. 4 presents the FD rate gain with varying number of antennas, $N \in \{4, 8, \ldots, 128\}$, and the *normalized* optimal FD TxBF and RxBF gain $g^\star/N \in [0, 1]$ (recall from (5) that $g_{\mathrm{t}}^{\max} = g_{\mathrm{r}}^{\max} = N$).

Fig. 4 shows, for example, that a 16-element FD phased array can achieve FD rate gains of 1.14/1.56/1.71× in low/medium/high SNR regimes, with 3 dB TxBF and RxBF gain loss (i.e., $g^\star = N/2$). These rate gains increase to 1.36/1.64/1.75× when $N = 64$. Moreover, with 6 dB TxBF and RxBF gain losses, a 64-element FD phased array can achieve FD rate gains of 1.05/1.46/1.62× in low/medium/high SNR regimes. As we will show in Section VII, a TxBF and RxBF gain loss of 6 dB is sufficient to achieve $\gamma_{bb}(f_k) \le 1, \forall k$, in most considered scenarios. It is also interesting to note that under sufficient link SNR values, an FD phased array with more antennas provides marginal improvements on the FD rate gain. For example, in the medium SNR regime, $N = 64/128$ elements can achieve FD rate gains of 1.64/1.67×, respectively (namely, doubling the number of antennas provides an improvement of only 3%).

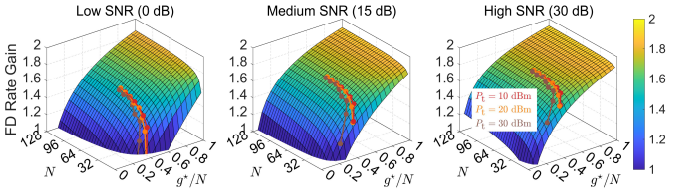

Fig. 6: FD rate gain in the BS-BS case with varying number of antennas, N, and the normalized optimal equal FD TxBF and RxBF gain, $g^\star/N$, for different link SNR values $\gamma \in \{0, 15, 30\}$ dB. The relationships between $g^\star/N$ and N, based on the Argos traces [13], are also overlayed on the surface with $P_{\mathrm{t}} \in \{10, 20, 30\}$ dBm.

To provide a practical example of the FD rate gain, we overlay in Fig. 4 curves that represent relationships between $g^\star/N$ and N using $\mathbf{H}(f_k)$ from the Argos dataset [13] with different Tx power levels (the details will be described in Section VII-D and shown in Fig. 11). For example, the Argos array with $P_{\mathrm{t}} = 20$ dBm can achieve $g^\star/N = 0.45/0.49/0.50$ for $N = 18/36/72$. In addition, the Argos array with $P_{\mathrm{t}} = 20$ dBm and $N = 36$ experiences only 3.1 dB TxBF and RxBF gain losses each, and can achieve maximum FD rate gains of 1.27/1.60/1.72× in low/medium/high SNR regimes. Importantly, the curves show that for a *given FD phased array* with given values of N and P_{t}, as well as the array geometry, there exists an upper limit of $g^\star$ on g_{t} and g_{r} that *any* FD Tx and Rx beamformers cannot exceed. The corresponding TxBF and RxBF gain losses are due to the SI that needs to be canceled leveraging TxBF and RxBF DoF to ensure FD operation in a phased array (otherwise a phased array can always achieve $g^\star = N$ in the HD mode). Since the FD rate gain increases as a function of $g^\star$ (see (13)–(14)), designing FD Tx and Rx beamformers that reach the upper limit of $g^\star$ will result in the maximum achievable FD rate gain.

We also evaluate the FD rate gain with asymmetric UL and DL SNR values, a scenario which is more common in realistic network settings. Fig. 5 presents the FD rate gain with varying UL and DL SNR values, γ_{bu} and γ_{ub}, with $N \in \{9, 36, 72\}$ and with 3 dB TxBF and RxBF gain loss. The results show that FD rate gains of 1.28–1.74×/1.37–1.75× can be achieved with $N = 36/72$ under all considered UL and DL SNR values. Note that the FD rate gain also increases as a function of the number of antennas, N.

BS-BS Case: Fig. 6 plots the FD rate gain in the BS-BS case with the same setting as used in the BS-User case. The results show that a 16-element FD phased array can achieve FD rate

gains of 1.25/1.53/1.66× in low/medium/high SNR regimes, with only 3 dB TxBF and RxBF gain loss. These gains increase to 1.49/1.64/1.72× with $N = 64$. The curves representing the relationships between $g^\star/N$ and N using the Argos traces are overlayed in Fig. 6, and similar observations as in the BS-User case are also relevant in the BS-BS case. In both use cases, the FD rate gain does not approach 2×, due to the XINR at the BS and user, $\gamma_{bb} = \gamma_{uu} = 1$.

Findings. As indicated above, although an FD phased array experiences TxBF and RxBF gain losses in the desired beam-pointing directions to achieve $\gamma_{bb}(f_k) \leq 1, \forall k$, the network can still achieve significant FD rate gains in various settings. Hence, it is important to obtain the optimal equal TxBF and RxBF gain, $g^\star$, in an FD phased array in order to achieve high FD rate gain in the considered use cases. The results also reveal an interesting phenomenon: with increased number of antennas, N, minimal TxBF and RxBF gain losses (e.g., 3 dB) do not affect the achieved FD rate gains. In addition, higher TxBF and RxBF gain losses are needed to achieve sufficient SIC under different Tx power level, P_{t}, and bandwidth, B, requirements, as we will show in Section VII. This tradeoff opens up a possibility of designing FD phased arrays with different geometries and/or values of N under varying system requirements (e.g., Tx power levels, link SNRs, bandwidth).

VI. Formulation and Optimization

In this section, we formulate an optimization problem based on the FD link objective described in Section IV-D. Due to the non-convexity and computational complexity of the problem, we then present an alternative formulation whose solution can be efficiently obtained using an iterative algorithm with provable performance guarantees.

A. Problem Formulation

Given the FD link objective in Section IV-D, the following problem jointly determines the FD Tx and Rx beamformers.

$$\textsf{(Opt-TxRx)}\ g^\star := \max\nolimits_{\mathbf{w},\mathbf{v}}\ g \tag{16}$$

$$\text{s.t.}: |\mathbf{s}_{\text{t}}^\top \mathbf{w}|^2/N = g,\ |\mathbf{s}_{\text{r}}^\top \mathbf{v}|^2/N = g, \tag{17}$$

$$P_{\text{SI}}^{\text{bf}}(f_k) = |\mathbf{v}^\top \mathbf{H}(f_k)\mathbf{w}|^2 \cdot \tfrac{P_{\text{t}}}{N} \leq N\beta,\ \forall k, \tag{18}$$

$$|w_n|^2 \leq 1,\ |v_n|^2 \leq 1,\ \forall n. \tag{19}$$

Specifically, the objective (16) is to maximize the TxBF and RxBF gains, subject to the following constraints (see Section IV-D): (i) the TxBF and RxBF gains in the desired beam-pointing directions, $(\phi_{\text{t}}, \theta_{\text{t}})$ and $(\phi_{\text{r}}, \theta_{\text{r}})$, are maximized[4], (17) (see also (4)), (ii) the residual SI power at any frequency is suppressed to below the array noise floor, i.e., $\gamma_{bb}(f_k) \leq 1, \forall k$, (18), and (iii) the amplitude of the beamforming weight on each Tx/Rx element is at most one (see Section III), (19). *Essentially, the Tx and Rx beamformers that are obtained as a solution are different from the conventional HD beamfomers such that the total SI power is canceled to below the array noise floor with minimal TxBF and RxBF gain loss*. In order words, TxBF and RxBF are *repurposed* for achieving wide-band RF SIC. We note that (Opt-TxRx) can also be extended to include general complex-valued desired array patterns. Throughout the paper, we practically set $P_{\text{nf}} = -90\,\text{dBm}$ and $SIC_{\text{dig}} = 40\,\text{dB}$.[5] According to (15), $\beta = P_{\text{nf}} \cdot SIC_{\text{dig}} = -90\,\text{dBm} + 40\,\text{dB} = -50\,\text{dBm} = 10^{-5}\,\text{mW}$.

Note that (17) and (19) are convex non-linear constraints, and (Opt-TxRx) always has a feasible solution where $\mathbf{w}$ and $\mathbf{v}$ have very small amplitudes. However, in general, (Opt-TxRx) is a *non-convex* optimization problem whose solution poses several challenges. The non-convexity stems from the coupling between $\mathbf{w}$ and $\mathbf{v}$ through $\mathbf{H}(f_k)$ in (18) where $\mathbf{H}(f_k)$ is not a Hermitian matrix, and not even a symmetric matrix in realistic environments (see Section IV-A). Moreover, the problem becomes computationally expensive to solve using existing solvers (which may only return a local optimum) with increased number of antennas, N, especially for massive-antenna systems and large-scale phased arrays. For benchmarking purposes, in Section VII, we use the nonlinear programming solver from MATLAB to solve (Opt-TxRx) and denote the returned (possibly only locally) optimal FD TxBF and RxBF gains by $g_{\text{t}}^\star$ and $g_{\text{r}}^\star$, respectively.[6]

TABLE I: Average accuracy of (Opt-TxRx-Relaxed) compared to (Opt-TxRx-Relaxed) with the obtained $a^\star$ and $g^\star$, respectively.

Number of antennas, N	9	18	27	36	≥ 45
$\left\lvert\frac{g^\star-(a^\star)^2/N}{g^\star}\right\rvert \times 100\%$ (%)	4.43	4.57	3.58	1.49	≤ 4.86

B. Observation and Intuition

Due to the intractability of (Opt-TxRx), we now describe alternative optimization problems which are based on the observations below. First, we relax (Opt-TxRx) into the following optimization problem by relaxing the quadratic constraint (17) given the linear relationship between the array factors and beamformers (see (4)),

$$\textsf{(Opt-TxRx-Relaxed)}\ a^\star := \max\nolimits_{\mathbf{w},\mathbf{v}}\ a$$
$$\text{s.t.}: \mathbf{s}_{\text{t}}^\top \mathbf{w} = a \in \mathbb{R}^+,\ \mathbf{s}_{\text{r}}^\top \mathbf{v} = a \in \mathbb{R}^+,\ \text{and (18)–(19)}.$$

In particular, the objective $\{\max_{\mathbf{w},\mathbf{v}} : a\}$ is equivalent to $\{\max_{\mathbf{w},\mathbf{v}} : g\}$ in (16), since the TxBF/RxBF gain, $g_{\text{t/r}}$, is a monotonically increasing function of real-valued, non-negative Tx/Rx array factors, $a_{\text{t/r}} \in \mathbb{R}^+$ (i.e., $g_{\text{t/r}} = a_{\text{t/r}}^2/N$, see (4)).

Using the Argos dataset [13] (described in Section VII-D) with different values of N and P_{t}, we numerically evaluated and confirmed that equal FD TxBF and RxBF gain obtained by solving (Opt-TxRx) and (Opt-TxRx-Relaxed), $g^\star$ and $(a^\star)^2/N$, respectively, have a relative difference of only within 5% in all considered scenarios. The results are presented in Table I and show the accuracy of (Opt-TxRx-Relaxed) as an approximation to (Opt-TxRx).

[4]This constraint can be easily modified to consider multiple Tx and Rx beam-pointing directions suitable for network scenarios with multiple users.

[5]Recent work has achieved $SIC_{\text{dig}} = 43/50\,\text{dB}$ [5], [8] which leads to more relaxed requirements on the amount of RF SIC.

[6]Due to the non-convexity of (Opt-TxRx), we use the same $g_{\text{t}}^\star$ and $g_{\text{r}}^\star$ as in Section IV-B to denote the numerically obtained solution to (Opt-TxRx) using existing solvers.

Second, note that the SI power in (18) can be written as,

$$\begin{aligned} P_{\text{SI}}^{\text{bf}}(f_k) &= |\mathbf{v}^\top \mathbf{H}(f_k)\mathbf{w}|^2 \cdot \tfrac{P_{\text{t}}}{N} \\ &= \left(\mathbf{v}^\top \mathbf{H}(f_k)\mathbf{w}\right)^\dagger \cdot \left(\mathbf{v}^\top \mathbf{H}(f)\mathbf{w}\right) \cdot \tfrac{P_{\text{t}}}{N} \\ &= \mathbf{w}^\dagger \Big(\underbrace{\mathbf{H}^\dagger(f_k)\mathbf{v}^*\mathbf{v}^\top \mathbf{H}(f_k)}_{:=\mathbf{H}_{\mathbf{v}}(f_k)} \Big) \mathbf{w} \cdot \tfrac{P_{\text{t}}}{N} \\ &= \mathbf{w}^\top \mathbf{H}_{\mathbf{v}}(f_k)\mathbf{w} \cdot \tfrac{P_{\text{t}}}{N}, \ \forall k. \end{aligned}$$

It can be seen that with a *fixed* Rx beamformer, $\mathbf{v}$,

- $\mathbf{H}_{\mathbf{v}}(f_k)$ is a *Hermitian* matrix, i.e., $\mathbf{H}_{\mathbf{v}}(f_k) = \mathbf{H}_{\mathbf{v}}^\dagger(f_k), \forall k$;
- $\mathbf{H}_{\mathbf{v}}(f_k)$ is *positive semidefinite* since, for any non-zero Tx beamformer, $\mathbf{w}$, the SI power cannot be negative, i.e.,

$$\mathbf{w}^\dagger \mathbf{H}_{\mathbf{v}}(f_k)\mathbf{w} \cdot \tfrac{P_{\text{t}}}{N} \geq 0, \ \forall k, \ \forall \mathbf{w} \in \mathbb{C}^N \text{ and } \mathbf{w} \neq \mathbf{0}.$$

Therefore, based on this observation and (Opt-TxRx-Relaxed), the optimal Tx beamformer that maximizes the Tx array factor, a_{t}, given a fixed $\mathbf{v}$, can be obtained by solving:

$$\begin{aligned} \text{(P1)} \ & \max_{\mathbf{w}} \ a_{\text{t}} \\ \text{s.t.} : \ & \mathsf{Re}[\mathbf{s}_{\text{t}}^\top \mathbf{w}] = a_{\text{t}}, \ \mathsf{Im}[\mathbf{s}_{\text{t}}^\top \mathbf{w}] = 0, \\ & \mathbf{w}^\dagger \mathbf{H}_{\mathbf{v}}(f_k)\mathbf{w} \cdot \tfrac{P_{\text{t}}}{N} \leq N\beta, \ \forall k, \ |w_n|^2 \leq 1, \ \forall n. \end{aligned}$$

Unlike (Opt-TxRx) and (Opt-TxRx-Relaxed), this is a *quadratically constrained convex program*, since $\mathbf{H}_{\mathbf{v}}(f_k)$ is a Hermitian matrix. Symmetrically, the optimal Rx beamformer that maximizes the Rx array factor given a fixed Tx beamformer $\mathbf{w}$, can be obtained by solving:

$$\begin{aligned} \text{(P2)} \ & \max_{\mathbf{v}} \ a_{\text{r}} \\ \text{s.t.} : \ & \mathsf{Re}[\mathbf{s}_{\text{r}}^\top \mathbf{v}] = a_{\text{r}}, \ \mathsf{Im}[\mathbf{s}_{\text{r}}^\top \mathbf{v}] = 0, \\ & \mathbf{v}^\dagger \mathbf{H}_{\mathbf{w}}(f_k)\mathbf{v} \cdot \tfrac{P_{\text{t}}}{N} \leq N\beta, \ \forall k, \ |v_n|^2 \leq 1, \ \forall n. \end{aligned}$$

(P1) and (P2) are convex programs that can be solved efficiently via existing solvers (e.g., CVX). Intuitively, an algorithm that updates $\mathbf{w}$ and $\mathbf{v}$ by iteratively solving (P1) and (P2) can be applied, i.e., solving for $\mathbf{v}$ given fixed $\mathbf{w}$, and then solving for an updated $\mathbf{w}$ with the newly obtained $\mathbf{v}$. However, the obtained TxBF and RxBF gains can be largely imbalanced since $\mathbf{w}$ and $\mathbf{v}$ are updated *independently*.

C. The Iterative Algorithm

We now present an iterative algorithm (described in Algorithm 1) that *simultaneously* maximizes and balances the Tx and Rx array factors.[7] Let $\kappa \in \mathbb{Z}$ be the index of iteration. Let $\mathbf{w}^{(0)}$ and $\mathbf{v}^{(0)}$ be the initial Tx and Rx beamformers with corresponding Tx and Rx array factors of $a_{\text{t}}^{(0)}$ and $a_{\text{r}}^{(0)}$, respectively. Let $\mathbf{w}^{(\kappa)}$ and $a_{\text{t}}^{(\kappa)}$ (resp. $\mathbf{v}^{(\kappa)}$ and $a_{\text{r}}^{(\kappa)}$) be the optimal Tx (resp. Rx) beamformer and Tx (resp. Rx) array factor obtained by the iterative algorithm in the κ^{th} iteration. For $\kappa \in \mathbb{Z}$, we define the following two objective functions.

$$\begin{aligned} F_{\text{t}}^{(\kappa+1)}(a_{\text{t}}) &= a_{\text{t}} - \alpha_{\kappa+1} \cdot (a_{\text{t}} - a_{\text{r}}^{(\kappa)})^2, \\ F_{\text{r}}^{(\kappa+1)}(a_{\text{r}}) &= a_{\text{r}} - \alpha_{\kappa+1} \cdot (a_{\text{r}} - a_{\text{t}}^{(\kappa+1)})^2, \end{aligned} \tag{20}$$

[7]The idea of the iterative algorithm is similar to that presented in [36].

Algorithm 1 The Iterative Algorithm

Input and Initialization: N, P_{t}, $\mathbf{H}(f_k), \forall k$, $\mathbf{s}_{\text{t}} = \mathbf{s}(\phi_{\text{t}}, \theta_{\text{t}})$, and $\mathbf{s}_{\text{r}} = \mathbf{s}(\phi_{\text{r}}, \theta_{\text{r}})$. Initial values of Tx and Rx beamformers $\mathbf{w}^{(0)}$ and $\mathbf{v}^{(0)}$, respectively. The step size sequence, $\{\alpha_\kappa\}_{\kappa \in \mathbb{Z}}$.

For $\kappa = 0, 1, \cdots$ **do**

1: Obtain $\mathbf{w}^{(\kappa+1)}$ with given $\mathbf{v}^{(\kappa)}$ and $a_{\text{r}}^{(\kappa)}$ by solving the following optimization problem, (Opt-Tx):

$$\begin{aligned} a_{\text{t}}^{(\kappa+1)} := \arg\max_{\mathbf{w}} \ & F_{\text{t}}^{(\kappa+1)}(a_{\text{t}}) = a_{\text{t}} - \alpha_{\kappa+1} \cdot (a_{\text{t}} - a_{\text{r}}^{(\kappa)})^2 \\ \text{s.t.} : \ & \mathsf{Re}[\mathbf{s}_{\text{t}}^\top \mathbf{w}] = a_{\text{t}}, \ \mathsf{Im}[\mathbf{s}_{\text{t}}^\top \mathbf{w}] = 0, \\ & \mathbf{w}^\dagger \mathbf{H}_{\mathbf{v}^{(\kappa)}}(f_k)\mathbf{w} \cdot \tfrac{P_{\text{t}}}{N} \leq N\beta, \ \forall k, \\ & |w_n|^2 \leq 1, \ \forall n. \end{aligned}$$

2: Obtain $\mathbf{v}^{(\kappa+1)}$ with given $\mathbf{w}^{(\kappa+1)}$ and $a_{\text{t}}^{(\kappa+1)}$ by solving the following optimization problem, (Opt-Rx):

$$\begin{aligned} a_{\text{r}}^{(\kappa+1)} := \arg\max_{\mathbf{v}} \ & F_{\text{r}}^{(\kappa+1)}(a_{\text{r}}) = a_{\text{r}} - \alpha_{\kappa+1} \cdot (a_{\text{r}} - a_{\text{t}}^{(\kappa+1)})^2 \\ \text{s.t.} : \ & \mathsf{Re}[\mathbf{s}_{\text{r}}^\top \mathbf{v}] = a_{\text{r}}, \ \mathsf{Im}[\mathbf{s}_{\text{r}}^\top \mathbf{v}] = 0, \\ & \mathbf{v}^\dagger \mathbf{H}_{\mathbf{w}^{(\kappa+1)}}(f_k)\mathbf{v} \cdot \tfrac{P_{\text{t}}}{N} \leq N\beta, \ \forall k, \\ & |v_n| \leq 1, \ \forall n. \end{aligned}$$

3: Iterate until the Tx and Rx array factor improvements are within δN, i.e.,

$$\max\left\{a_{\text{t}}^{(\kappa+1)} - a_{\text{t}}^{(\kappa)}, a_{\text{r}}^{(\kappa+1)} - a_{\text{r}}^{(\kappa)}\right\} \leq \delta \cdot N. \tag{22}$$

Output: $\mathbf{w}^{(\kappa+1)}$, $\mathbf{v}^{(\kappa+1)}$, and the corresponding TxBF and RxBF gains, $g_{\text{t}}^{(\kappa+1)} = (a_{\text{t}}^{(\kappa+1)})^2/N$ and $g_{\text{r}}^{(\kappa+1)} = (a_{\text{r}}^{(\kappa+1)})^2/N$.

where $\alpha_{\kappa+1}$ is the *step size*. Essentially, in the $(\kappa+1)^{\text{th}}$ iteration, a penalty term is introduced, which is the square of the difference between the Tx and Rx array factors with a weighting factor of $\alpha_{\kappa+1}$. Therefore, Tx and Rx array factors with a larger difference will prevent their individual value from increasing rapidly.

To allow analytical tractability and easy implementation of the developed iterative algorithm, it is important to properly select: (i) the initial Tx and Rx beamformers, $\mathbf{w}^{(0)}$ and $\mathbf{v}^{(0)}$, and (ii) the step size sequence, $\{\alpha_\kappa\}_{\kappa \in \mathbb{Z}}$. In particular, we set:

$$\mathbf{w}^{(0)} = \tfrac{\beta^{1/4} \cdot \mathbf{w}_{\text{conv}}}{2P_{\text{t}}^{1/4} N^{1/2}}, \ \mathbf{v}^{(0)} = \tfrac{\beta^{1/4} \cdot \mathbf{v}_{\text{conv}}}{2P_{\text{t}}^{1/4} N^{1/2}}, \ \alpha_\kappa = \tfrac{1}{\kappa^2}, \ \forall \kappa, \tag{21}$$

since this choice of $\mathbf{w}^{(0)}$ and $\mathbf{v}^{(0)}$ satisfies (18), i.e.,

$$\begin{aligned} & |(\mathbf{v}^{(0)})^\top \mathbf{H}(f_k)\mathbf{w}^{(0)}|^2 \cdot \tfrac{P_{\text{t}}}{N} \\ & \leq \left[\tfrac{\beta^{1/4}}{2P_{\text{t}}^{1/4} N^{1/2}}\right]^4 \cdot |\mathbf{v}_{\text{conv}}|^2 \cdot |\mathbf{w}_{\text{conv}}|^2 \cdot \tfrac{P_{\text{t}}}{N} = \tfrac{1}{2} \cdot N\beta < N\beta. \end{aligned}$$

We also note that the above choices of $\mathbf{w}^{(0)}$, $\mathbf{v}^{(0)}$, and $\{\alpha_\kappa\}$ are *not unique*. For example, any step size sequence $\{\alpha_\kappa\}$ satisfying $1 = \alpha_1 \geq \alpha_2 \geq \cdots > 0$ also suffices. In Section VII, we will evaluate the effect of $\{\alpha_\kappa\}$ on the solution obtained by the iterative algorithm.

D. Performance Analysis

In this section, we analyze the performance of the iterative algorithm. We first present Lemma 6.1 about the structural properties of the objective functions of (Opt-Tx) and (Opt-Rx) in (20). Then, we state the main results in Proposition 6.2. The proofs of Lemma 6.1 and Proposition 6.2 can be found in Appendices A and B, respectively.

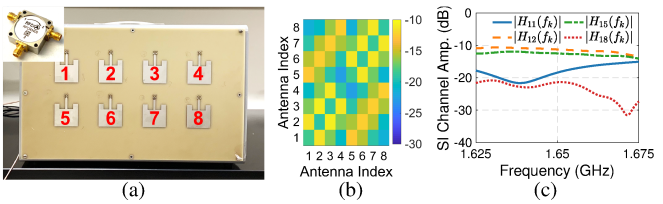

(a) (b) (c)

Fig. 7: (a) A customized 1.65 GHz 8-element rectangular array and the RFCR3206 circulator, (b) the measured $|H_{mn}(f_k)|$ at 1.65 GHz, and (c) the amplitudes of some example SI channels, $|H_{mn}(f_k)|$.

Lemma 6.1. *Under the iterative algorithm,* $\forall \kappa \in \mathbb{Z}$,

$$F_t^{(\kappa+1)}(a_t^{(\kappa+1)}) \geq F_t^{(\kappa+1)}(a_t^{(\kappa)}),$$
$$F_r^{(\kappa+1)}(a_r^{(\kappa+1)}) \geq F_r^{(\kappa+1)}(a_r^{(\kappa)}).$$

Recall that $g_{\mathrm{t}}^{(\kappa)} = (a_{\mathrm{t}}^{(\kappa+1)})^2/N$ and $g_{\mathrm{r}}^{(\kappa)} = (a_{\mathrm{r}}^{(\kappa+1)})^2/N$. We have the following proposition.

Proposition 6.2. *With initial Tx and Rx beamformers,* $\mathbf{w}^{(0)}$ *and* $\mathbf{v}^{(0)}$*, and step size,* α_κ*, given in* (21)*, under the iterative algorithm,*

$$a_t^{(\kappa+1)} \geq a_t^{(\kappa)} \text{ and } a_r^{(\kappa+1)} \geq a_r^{(\kappa)}, \ \forall \kappa \in \mathbb{Z}. \tag{23}$$

Furthermore, the corresponding TxBF and RxBF gains satisfy, $\forall \kappa \in \mathbb{Z}$,

$$g_t^{(\kappa+1)} \geq g_t^{(\kappa)}, \ g_t^{(\kappa+1)} \geq g_r^{(\kappa)}, \ g_t^{(\kappa+1)} + g_r^{(\kappa+1)} \geq g_t^{(\kappa)} + g_r^{(\kappa)}. \tag{24}$$

Corollary 6.1. *The iterative algorithm is guaranteed to terminate in at most* $\lceil 1/\delta \rceil$ *iterations.*

Proof. Proposition 6.2 states that the Tx and Rx array factors obtained by Algorithm 1 after each iteration, $a_{\mathrm{t}}^{(\kappa)}$ and $a_{\mathrm{r}}^{(\kappa)}$, are always *monotonically non-decreasing*. From the termination condition (22) and the fact that $a_{\mathrm{t}}^{\max} = a_{\mathrm{r}}^{\max} = N$ (see (5)), the iterative algorithm is guaranteed to terminate within at most $\lceil N/(\delta \cdot N) \rceil = \lceil 1/\delta \rceil$ iterations. □

VII. Measurement-based Evaluation

In this section, we first describe the measurements, datasets, and setup. Then, we numerically evaluate the performance of an FD phased array with TxBF and RxBF, and the corresponding FD rate gains. We also discuss various design tradeoffs.

A. Measurements and Datasets

Since currently large-scale Tx and Rx phased array nodes are not widely available, our evaluations are based on $\mathbf{H}(f_k)$ from measurements and traces with different bandwidth, B. In particular, we consider two antenna arrays with different array geometries, number of antennas, and operating frequencies.

A Customized Rectangular Array with Circulators. We custom designed a 1.65 GHz 8-element rectangular antenna array using a slot loop antenna structure as shown in Fig. 7(a). The spacing between adjacent antennas is half-wavelength. An RF-CI RFCR3406 circulator is also included (see Fig. 3). The frequency responses of the antenna array and the circulator are measured using a vector network analyzer at frequencies between 1.625–1.675 GHz ($B = 50$ MHz), from which the SI channel matrix, $\mathbf{H}(f_k) \in \mathbb{C}^{8\times 8}$, is constructed. Figs. 7(b) and 7(c) respectively plot the measured $|H_{mn}(f_k)|$ at $f_k = 1.65$ GHz, and example SI channels, $|H_{mn}(f_k)|$, with high frequency-selectivity.

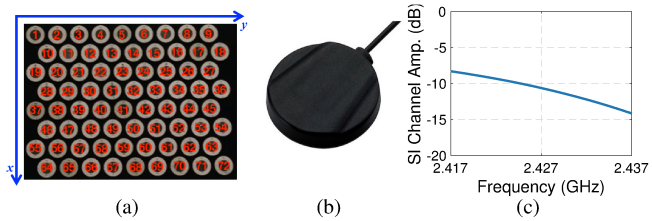

(a) (b) (c)

Fig. 8: (a) The 2.4 GHz 72-element Argos hexagonal array with SI channel measurements reported in [13], [30], (b) the Taoglas 2.4 GHz circular antenna, and (c) the measured antenna amplitude response used for $|H_{nn}(f_k)|, \forall n$.

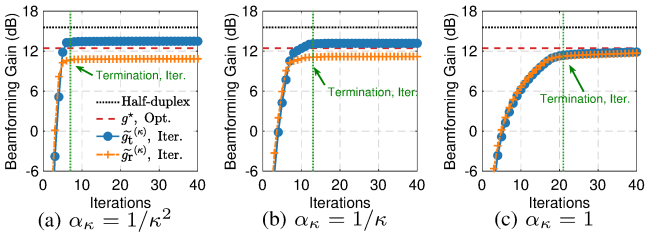

(a) $\alpha_\kappa = 1/\kappa^2$ (b) $\alpha_\kappa = 1/\kappa$ (c) $\alpha_\kappa = 1$

Fig. 9: The optimal TxBF and RxBF gain, $g^\star$, and the TxBF and RxBF gains obtained the by iterative algorithm, $\widetilde{g}_{\mathrm{t}}^{(\kappa)}$ and $\widetilde{g}_{\mathrm{r}}^{(\kappa)}$, with $N = 36$, $P_{\mathrm{t}} = 20$ dBm, and different step sizes, $\{\alpha_\kappa\}$.

The Argos Hexagonal Array [13], [14]. We also leverage the publicly available Argos dataset from [13], [14]. The Argos platform consists of 72 circular patch antennas at 2.4 GHz placed in a hexagonal grid consisting of 8 rows and 9 columns, with 0.6-wavelength spacing between adjacent elements (see Fig. 8(a)). The SI channel matrix, $\mathbf{H}(f_k) \in \mathbb{C}^{72\times 72}$, is measured using a WARPv3 platform with $B = 20$ MHz bandwidth and $K = 64$ subcarriers (52 non-zero subcarriers). With such a large number of antennas, uniform linear arrays (ULAs) and hexagonal planar arrays with different values of N can be constructed by taking a subset of the measurements.

However, the Argos platform employs *seperate* Tx and Rx antennas and does not contain circulators. Therefore, $\mathbf{H}(f_k)$ is missing the diagonal elements, $H_{nn}(f_k), \forall n$. To complete $\mathbf{H}(f_k)$, we measure the frequency response of a Taoglas 2.4 GHz circular antenna (see Fig. 8(b)). Using the completed $\mathbf{H}(f_k)$, we generate hexagonal arrays with $N \in \{9, \ldots, 72\}$ by considering the top $\{1, \ldots, 8\}$ rows of the Argos array. Note that case of $N = 9$ corresponds to a ULA.

Steering Vectors of the Rectangular and Argos Arrays. The steering vector of the rectangular array is computed as described in Section III. The steering vector of the Argos hexagonal array is given by $(n = (n_x - 1)N_y + n_y)$

$$s_n(\phi, \theta) = \begin{cases} e^{j\frac{6\pi}{5}[(n_x-1)\cos\theta\cos\phi + \frac{\sqrt{3}}{2}(n_y-1)\cos\theta\sin\phi]}, & n_y \text{ odd}, \\ e^{j\frac{6\pi}{5}[(n_x-\frac{1}{2})\cos\theta\cos\phi + \frac{\sqrt{3}}{2}(n_y-1)\cos\theta\sin\phi]}, & n_y \text{ even}. \end{cases}$$

Our evaluations using the Argo dataset is with 20 MHz as provided [13], [14]. For higher bandwidth up to 50 MHz, we use the rectangular array measurements. For compactness of presentation, we use $N \in \{8, 9, 18, \ldots, 72\}$ to correspond to different array geometries. Note that in both antenna arrays,

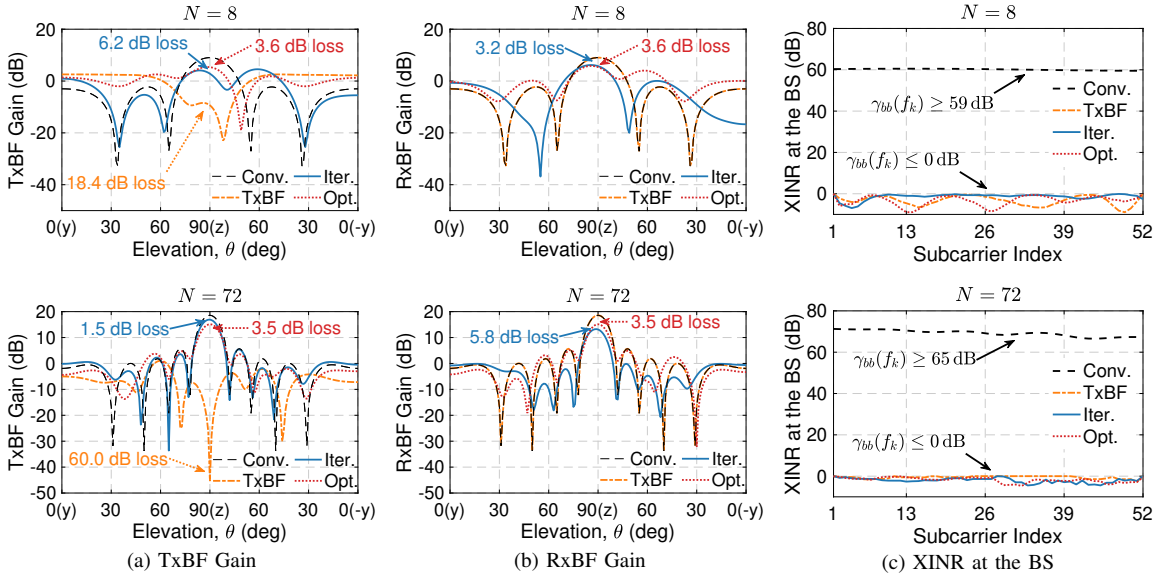

(a) TxBF Gain (b) RxBF Gain (c) XINR at the BS

Fig. 10: TxBF and RxBF gains (on the y-z plane), and the resulting XINR under different TxBF and RxBF schemes with the rectangular array ($N = 8$) and the Argos array ($N = 72$), $P_{\mathrm{t}} = 30\,\mathrm{dBm}$, $B = 20\,\mathrm{MHz}$, and the Tx and Rx beam-pointing directions in the array broadside (z-axis).

the measured $\mathbf{H}(f_k)$ is neither Hermitian nor symmetric although Fig. 7(b) presents some level of symmetry.

B. Setup

TxBF and RxBF in HD and FD Modes. We consider TxBF and RxBF in the *front side* of the antenna array with $\phi \in [-180°, 180°]$ and $\theta \in [0°, 90°]$. Specifically, the array *broadside* corresponds to the direction of $\theta = 90°, \forall \phi$ (see Fig. 2(a)). We consider $P_{\mathrm{t}} \in \{10, 20, 30\}\,\mathrm{dBm}$[8], and $P_{\mathrm{nf}} = -90\,\mathrm{dBm}$ and $SIC_{\mathrm{dig}} = 40\,\mathrm{dB}$ (see Section IV-D). The FD rate gains are computed as described in Section IV-C.

The following TxBF and RxBF schemes are considered:

(1) *Conventional HD TxBF and RxBF* (**Conv.**), which is based on (5) and $g_{\mathrm{t}}^{\max} = g_{\mathrm{r}}^{\max} = N$;

(2) *Only TxBF* (**TxBF**), which is similar to the approach presented in [32] but adapted to our FD phased array model (see Section IV). Since [32] considers a narrowband system where only TxBF is repurposed, we set the Rx beamformer in this scheme to be $\mathbf{v}_{\mathrm{conv}}$, which maximizes the RxBF gain in the main beam-pointing direction, and optimize for the Tx beamformer across the desired wide bandwidth;

(3) *Optimal FD TxBF and RxBF* (**Opt.**), which is based on solving (Opt-TxRx). We denote the (equal) optimal TxBF and RxBF gain as $g^{\star}$;

(4) *Iterative FD TxBF and RxBF* (**Iter.**), which is based on the iterative algorithm (Algorithm 1) with $\delta = 0.01$ set in the termination step. We denote $\widetilde{g}_{\mathrm{t}}$ and $\widetilde{g}_{\mathrm{r}}$ as the obtained TxBF and RxBF) gains, respectively.

The evaluations are performed using a laptop with a quad-core Intel i7 CPU and 16 GB RAM. For **Opt.**, we apply the nonlinear solver in MATLAB.[9] For **Iter.**, we apply the MATLAB CVX solver for solving the convex (Opt-Tx) and (Opt-Rx) in Algorithm 1. For **TxBF**, we also apply the CVX solver given the convexity of the optimization problem.

Selecting the Step Size, $\{\alpha_\kappa\}$. To study the impact of $\{\alpha_\kappa\}$, we remove the termination condition in the iterative algorithm and record the obtained $a_{\mathrm{t}}^{(\kappa)}$ and $a_{\mathrm{r}}^{(\kappa)}$ (see Algorithm 1). We consider $N = 36$, $P_{\mathrm{t}} = 20\,\mathrm{dBm}$, and three different step sizes satisfying the conditions specified in Section VI-C: (i) $\alpha_\kappa = 1/\kappa^2$, (2) $\alpha_\kappa = 1/\kappa$, and (iii) $\alpha_\kappa = 1$ (constant). Fig. 9 plots both the obtained $a_{\mathrm{t}}^{(\kappa)}$ and $a_{\mathrm{r}}^{(\kappa)}$ over iterations, κ, and the optimal Tx and Rx array factor, $a^{\star}$ (red dashed line). The results show that under all considered three choices of $\{\alpha_\kappa\}$, $a_{\mathrm{t}}^{(\kappa)}$ and $a_{\mathrm{r}}^{(\kappa)}$ converge within 25 iterations. However, $a_{\mathrm{t}}^{(\kappa)}$ and $a_{\mathrm{r}}^{(\kappa)}$ become more imbalanced with more aggressive step sizes (e.g., $\alpha_\kappa = 1/\kappa^2$). The results for other values of N and P_{t} also reveal similar trends. Therefore, we empirically set $\alpha_\kappa = 1/\kappa^2$, which achieves fast termination (e.g., less than 10 iterations for all values of N, P_{t}, and B considered). Note that the obtained $\widetilde{g}_{\mathrm{t}}$ and $\widetilde{g}_{\mathrm{r}}$ are less balanced compared with $\alpha_\kappa = 1/\kappa$ or $\alpha_\kappa = 1$.

C. XINR and Gain Loss under TxBF and RxBF

We now evaluate the XINR at the BS, $\gamma_{bb}(f_k)$, under different TxBF and RxBF schemes. We consider both the customized rectangular array ($N = 8$) and the Argos array ($N = 72$), with $P_{\mathrm{t}} = 30\,\mathrm{dBm}$, $B = 20\,\mathrm{MHz}$, and the desired Tx and Rx beam-pointing directions in the array broadside (z-axis). Fig. 10 plots the TxBF and RxBF gains (see (2)) and the resulting XINR, $\gamma_{bb}(f_k)$, under the considered TxBF and RxBF schemes. It can be seen that **Conv.** results in extremely

[8]These values correspond to the typical Tx power levels of a BS in a small/micro cell.

[9]The returned solution to (Opt-TxRx) may be locally optimal due to its non-convexity.

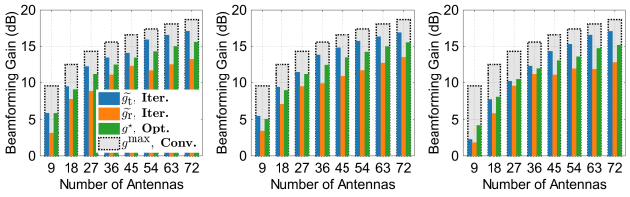

(a) $P_t = 10$ dBm (b) $P_t = 20$ dBm (c) $P_t = 30$ dBm

Fig. 11: TxBF and RxBF gains under different TxBF and RxBF schemes with varying number of antennas, N, and $P_t \in \{10, 20, 30\}$ dBm.

TABLE II: Average ratio between the FD rate gains achieved under **Iter.** (with $\widetilde{g}_t$ and $\widetilde{g}_r$) and **Opt.** (with $g^\star$).

Number of antennas, N	9	18	27	36	≥ 45
Low SNR (0 dB)	0.89	0.95	0.97	0.98	≥ 0.98
Medium SNR (15 dB)	0.93	0.97	0.98	0.99	≥ 0.99
High SNR (30 dB)	0.95	0.98	0.98	0.99	≥ 0.99

high XINR of $\gamma_{bb}(f_k) \geq 65$ dB, $\forall k$, thereby FD operation at the BS cannot be supported. Both **Opt.** and **Iter.** are able to cancel the SI power to below the array noise floor, i.e., $\gamma_{bb}(f_k) \leq 1$ (0 dB). The corresponding TxBF and RxBF gain losses under **Opt./Iter.** are only 3.6/6.2 dB and 3.6/3.2 dB for $N = 8$. The TxBF and RxBF gain losses are reduced to 3.5/1.5 dB and 3.5/5.8 dB for $N = 72$.

Fig. 10 also shows that the **TxBF** scheme leads to significantly higher TxBF gain losses of 18.4/60.0 dB for 8/72 elements, respectively, compared to the proposed **Opt.** and **Iter.** schemes. This is because with a *fixed* Rx beamformer that aims to achieve the maximum RxBF gain (as applied in **TxBF**), more attenuated Tx beamformer weights are required to cancel the strong SI. Therefore, we do not include **TxBF** in the rest of the evaluations since these largely degraded TxBF gains will lead to poor FD rate gains.

D. FD TxBF and RxBF Gains and Rate Gain

FD TxBF and RxBF Gains. We first evaluate the FD TxBF and RxBF gains. We consider Tx and Rx beam-point directions in the array broadside with $N \in \{9, 18, \ldots, 72\}$ and $P_t \in \{10, 20, 30\}$ dBm. Fig. 11 plots the optimal FD TxBF and RxBF gain, $g^\star$, and the iterative FD TxBF and RxBF gains, $\widetilde{g}_t$ and $\widetilde{g}_r$, respectively. The conventional HD TxBF and RxBF gains of N are also plotted. The results show that for a given number of antennas, N, the TxBF and RxBF gain losses are more significant with increased Tx power level, P_t. For a given value of P_t, the TxBF and RxBF gain losses decrease with a larger number of antennas, N. For example, under the **Iter.** scheme, an FD phased array with $P_t = 20$ dBm and $N = 72$ experiences 1.7/5.1 dB TxBF/RxBF gain losses, respectively. These values are only marginally changed to 1.8/5.7 dB with $N = 36$. It can also be seen that **Iter.** achieves relative balanced FD TxBF and RxBF gains across varying N. Specifically, $\widetilde{g}_t$ and $\widetilde{g}_r$ are always within ± 2.8 dB of the optimal FD TxBF and RxBF gain, $g^\star$. Moreover, $\gamma_{bb}(f_k) \leq 1, \forall k$, can be achieved with at most 8.0/8.2/11.6 dB *sum* TxBF and RxBF gain loss for $P_t = 10/20/30$ dBm when $N \geq 18$.

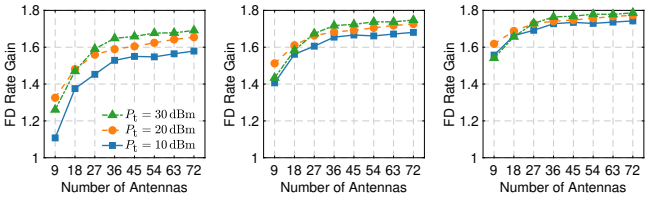

(a) Low SNR (0 dB) (b) Medium SNR (15 dB) (c) High SNR (30 dB)

Fig. 12: FD rate gain in the BS-BS case when both BSs face each other in the broadside, with varying number of antennas, N, and $P_t \in \{10, 20, 30\}$ dBm, in the low/medium/high SNR regimes.

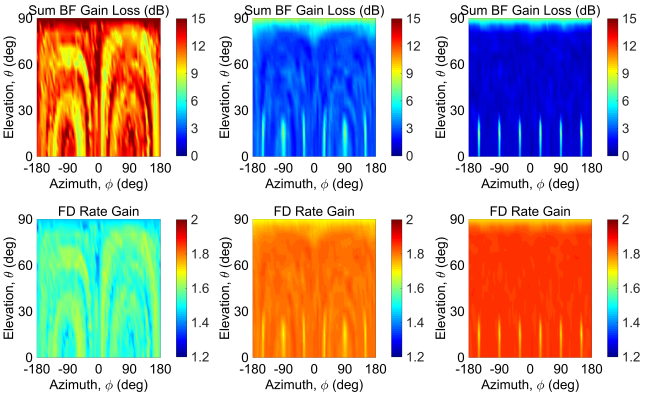

(a) $N = 9$ (b) $N = 36$ (c) $N = 72$

Fig. 13: Spatial distributions of the FD rate gain in the BS-User case when the user is in different spatial directions from the FD BS, with $N \in \{9, 36, 72\}$, $P_t = 30$ dBm, and $\gamma_{bu} = \gamma_{ub} = 0$ dB.

BS-BS Case. We consider the FD rate gain when both BSs face each other in the array broadside.[10] Fig. 12 plots the FD rate gains under the **Iter.** scheme with varying P_t and link SNR values. The results show that although the FD phased array experiences TxBF and RxBF gain losses to achieve $\gamma_{bb}(f_k) \leq 1, \forall k$, an FD rate gain of at least 1.53× can be achieved with $N \geq 36$ in all SNR regimes. Also, the FD rate gain improves with increased values of both N and the link SNR. Moreover, when the number of antennas is large, further increasing N introduces only marginal FD rate gain since the SI power is already canceled to below the noise floor with a smaller value of N (see Section V).

To compare the performance of the **Iter.** and **Opt.** schemes, Table II summarizes the average ratio between the FD rate gains achieved by **Iter.** (with $\widetilde{g}_t$ and $\widetilde{g}_r$) and **Opt.** (with $g^\star$). The results show that the FD rate gains achieved under $\widetilde{g}_t$ and $\widetilde{g}_r$ are very close to that achieved under $g^\star$, in all considered scenarios, where the average ratio is at least 89%.

BS-User Case with Spatially Distributed Users. We consider spatially distributed users in the directions of $\phi \in [-180°, 180°]$ and $\theta \in [0°, 90°]$ with respect to the BS. The BS applies the **Iter.** scheme with the desired Tx and Rx beam-pointing directions equal to the user direction. We consider the low SNR regime with $P_t = 30$ dBm and $N \in \{9, 36, 72\}$ (see Section V). Fig. 13 plots the spatial distributions of (i) the sum TxBF and RxBF gain loss for achieving $\gamma_{bb}(f_k) \leq 1, \forall k$ at the BS by the **Iter.** scheme, and (ii) the resulting FD rate

[10]Note that the proposed optimization and Algorithm 1 can also be applied to cases where the two BS do not face each other in the broadside.

TABLE III: Runtime improvements of the iterative algorithm over directly solving the non-convex (Opt-TxRx).

N	9	18	27	36	45	54	63	72
Runtime Impr.	0.99×	1.72×	2.41×	2.12×	2.70×	3.18×	5.51×	6.00×

gain with low UL and DL SNR values of 0 dB.

The results show that the sum TxBF and RxBF gain loss varies across all spatial directions, since the total SI power depends on both the array geometry and the beam-pointing directions. The SI power is the strongest (i.e., requiring the highest amount of RF SIC) in the array broadside (z-axis) and in the direction of adjacent antennas close to the array x-y plane (e.g., $\phi = \pm 90°$ for $N = 9$ and $\phi = \pm 30/90/150°$ for $N \in \{36, 72\}$, with very small values of θ). Yet, the **Iter.** scheme is still able to achieve $\gamma_{bb}(f_k) \leq 1$ (>65 dB RF SIC) under $P_{\mathrm{t}} = 30$ dBm with maximum sum TxBF and RxBF gain losses of 9.7/8.6 dB for $N = 36/72$. Overall, the FD rate gains are at least 1.33/1.66/1.68× for $N = 9/36/72$, and when the user is not in the direction of the strongest SI power, the FD rate gains can be increased to 1.68/1.83/1.87× for $N = 9/36/72$. Note that only 0 dB UL and DL SNR values are considered, and higher link SNR values would also increase FD rate gain at the same sum TxBF and RxBF gain loss.

Efficiency of the Iterative Algorithm. We also compare the performance of the **Iter.** and **Opt.** schemes in terms of the time consumed to obtain the Tx and Rx beamformers. We perform 100 runs of solving (Opt-TxRx) and of the iterative algorithm in all considered values of N and P_{t}, and measure the average running times. Table III summarizes the improvements in the average running time of **Iter.** over **Opt.**. The results show that with $N = 9$, both schemes have similar running times. However, as N increases, the **Iter.** scheme achieves 2–6× runtime improvements compared to the **Opt.** scheme, since the latter is solving the non-convex problem (Opt-TxRx).

Effect of the Bandwidth, B. Lastly, we evaluate the effects of the desired RF SIC bandwidth, B, on the FD TxBF and RxBF using the measurements of the 8-element rectangular array with circulators (recall that the Argos dataset is only with $B = 20$ MHz). We consider the **Iter.** scheme with $B \in \{10, \ldots, 50\}$ MHz and $P_{\mathrm{t}} \in \{10, 20, 30\}$ dBm. Fig. 14 plots the sum TxBF and RxBF gain loss and the corresponding FD rate gain in both the BS-User and BS-BS cases. The results show that, even with only 8 elements, an FD phased array can achieve $\gamma_{bb}(f_k) \leq 1, \forall k$, for up to $B = 50$ MHz at $P_{\mathrm{t}} = 10$ dBm, where the sum TxBF and RxBF gain loss is at most 8.5 dB (TxBF/RxBF gain loss of 4.4/4.1 dB). The sum TxBF and RxBF gain loss increases to 12.3 dB with $P_{\mathrm{t}} = 20$ dBm.[11] However, although higher TxBF and RxBF gain losses are required in scenarios with increased P_{t} and B, an 8-element FD phased array is able to achieve FD rate gains of at least 1.47/1.42/1.36× under $P_{\mathrm{t}} = 10/20/30$ dBm, with bandwidth of up to $B = 50$ MHz.

[11]The small variations on the curves are caused by the selection of the step size sequence of Algorithm 1, $\{\alpha_\kappa\}$.

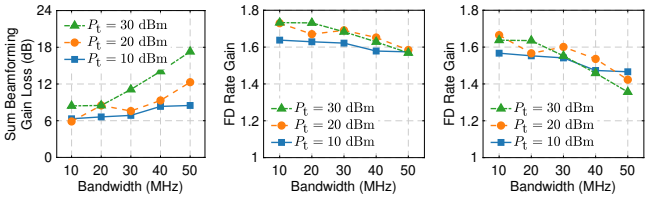

(a) Sum BF Gain Loss (b) The BS-User Case (c) The BS-BS Case

Fig. 14: Sum TxBF and RxBF gain loss, and FD rate gains in the BS-User and BS-BS cases with $N = 8$ and varying desired RF SIC bandwidth, $B \in \{10, \ldots, 50\}$ MHz, and $P_{\mathrm{t}} \in \{10, 20, 30\}$ dBm.

VIII. Conclusions

In this paper, we considered FD phased arrays repurposing TxBF and RxBF for achieving wideband RF SIC. We formulated optimization problems to obtain the maximum FD TxBF and RxBF gains and developed an iterative algorithm to efficiently solve the optimization problems. Using measurements and datasets, we extensively evaluated the performance of the FD phased array and the resulting FD rate gains in various network settings. Future directions include: (i) system design and implementation of a large-scale FD phased array based on our previous work [33], and its integration in the city-scale COSMOS testbed [16], [37], and (ii) experimental evaluation of the FD TxBF and RxBF approach, and its integration in hybrid beamforming systems and multi-user scenarios.

References

[1] T. Chen, M. B. Dastjerdi, H. Krishnaswamy, and G. Zussman, "Wideband full-duplex phased array with joint transmit and receive beamforming: Optimization and rate gains," in *Proc. ACM MobiHoc'19*, 2019.

[2] A. Sabharwal, P. Schniter, D. Guo, D. W. Bliss, S. Rangarajan, and R. Wichman, "In-band full-duplex wireless: Challenges and opportunities," *IEEE J. Sel. Areas Commun.*, vol. 32, no. 9, pp. 1637–1652, 2014.

[3] H. Krishnaswamy and G. Zussman, "1 chip 2x the bandwidth," *IEEE Spectrum*, vol. 53, no. 7, pp. 38–54, 2016.

[4] M. Duarte, C. Dick, and A. Sabharwal, "Experiment-driven characterization of full-duplex wireless systems," *IEEE Trans. Wireless Commun.*, vol. 11, no. 12, pp. 4296–4307, 2012.

[5] D. Bharadia, E. McMilin, and S. Katti, "Full duplex radios," in *Proc. ACM SIGCOMM'13*, 2013.

[6] M. Chung, M. S. Sim, J. Kim, D. K. Kim, and C.-B. Chae, "Prototyping real-time full duplex radios," *IEEE Commun. Mag.*, vol. 53, no. 9, pp. 56–63, 2015.

[7] J. Zhou, N. Reiskarimian, J. Diakonikolas, T. Dinc, T. Chen, G. Zussman, and H. Krishnaswamy, "Integrated full duplex radios," *IEEE Communn. Mag.*, vol. 55, no. 4, pp. 142–151, 2017.

[8] T. Chen, M. B. Dastjerdi, J. Zhou, H. Krishnaswamy, and G. Zussman, "Wideband full-duplex wireless via frequency-domain equalization: Design and experimentation," in *Proc. ACM MobiCom'19*, 2019.

[9] B. D. Van Veen and K. M. Buckley, "Beamforming: A versatile approach to spatial filtering," *IEEE ASSP Mag.*, vol. 5, no. 2, pp. 4–24, 1988.

[10] A. B. Constantine, *Antenna theory: Analysis and design, third edition*. John Wiley & Sons, 2005.

[11] D. Bharadia and S. Katti, "Full duplex MIMO radios," in *Proc. USENIX NSDI'14*, 2014.

[12] E. Aryafar, M. A. Khojastepour, K. Sundaresan, S. Rangarajan, and M. Chiang, "MIDU: Enabling MIMO full duplex," in *Proc. ACM MobiCom'12*, 2012.

[13] "Argos full-duplex channel measurement dataset," http://data.argos.rice.edu/, 2016.

[14] C. Shepard, H. Yu, N. Anand, E. Li, T. Marzetta, R. Yang, and L. Zhong, "Argos: Practical many-antenna base stations," in *Proc. ACM MobiCom'12*, 2012.

[15] K. E. Kolodziej, J. G. McMichael, and B. T. Perry, "Multitap RF canceller for in-band full-duplex wireless communications," *IEEE Trans. Wireless Commun.*, vol. 15, no. 6, pp. 4321–4334, 2016.

[16] T. Chen, M. Baraani Dastjerdi, J. Zhou, H. Krishnaswamy, and G. Zussman, "Open-access full-duplex wireless in the ORBIT testbed," *arXiv preprint arXiv:1801.03069v2*, 2018.

[17] J. Marasevic and G. Zussman, "On the capacity regions of single-channel and multi-channel full-duplex links," in *Proc. ACM MobiHoc'16*, 2016.

[18] M. Duarte, A. Sabharwal, V. Aggarwal, R. Jana, K. Ramakrishnan, C. W. Rice, and N. Shankaranarayanan, "Design and characterization of a full-duplex multiantenna system for WiFi networks," *IEEE Trans. Veh. Technol.*, vol. 63, no. 3, pp. 1160–1177, 2014.

[19] Y. Yang and N. B. Shroff, "Scheduling in wireless networks with full-duplex cut-through transmission," in *Proc. IEEE INFOCOM'15*, 2015.

[20] Y. Sun, D. W. K. Ng, Z. Ding, and R. Schober, "Optimal joint power and subcarrier allocation for full-duplex multicarrier non-orthogonal multiple access systems," *IEEE Trans. Commun.*, vol. 65, no. 3, pp. 1077–1091, 2017.

[21] Z. Qian, F. Wu, Z. Zheng, K. Srinivasan, and N. B. Shroff, "Concurrent channel probing and data transmission in full-duplex MIMO systems," in *Proc. ACM MobiHoc'17*, 2017.

[22] T. Chen, J. Diakonikolas, J. Ghaderi, and G. Zussman, "Hybrid scheduling in heterogeneous half-and full-duplex wireless networks," in *Proc. IEEE INFOCOM'18*, 2018.

[23] T. Riihonen, S. Werner, and R. Wichman, "Mitigation of loopback self-interference in full-duplex MIMO relays," *IEEE Trans. Signal Process.*, vol. 59, no. 12, pp. 5983–5993, 2011.

[24] H. A. Suraweera, I. Krikidis, G. Zheng, C. Yuen, and P. J. Smith, "Low-complexity end-to-end performance optimization in MIMO full-duplex relay systems," *IEEE Trans. Wireless Commun.*, vol. 13, no. 2, pp. 913–927, 2014.

[25] I. Krikidis, H. A. Suraweera, P. J. Smith, and C. Yuen, "Full-duplex relay selection for amplify-and-forward cooperative networks," *IEEE Trans. Wireless Commun.*, vol. 11, no. 12, pp. 4381–4393, 2012.

[26] L. Chen, F. Wu, J. Xu, K. Srinivasan, and N. Shroff, "Bipass: Enabling end-to-end full duplex," in *Proc. ACM MobiCom'17*, 2017.

[27] G. Zheng, I. Krikidis, J. Li, A. P. Petropulu, and B. Ottersten, "Improving physical layer secrecy using full-duplex jamming receivers," *IEEE Trans. Signal Process.*, vol. 61, no. 20, pp. 4962–4974, 2013.

[28] G. Sun, F. Wu, X. Gao, and G. Chen, "PHED: Pre-handshaking neighbor discovery protocols in full duplex wireless ad hoc networks," in *Proc. IEEE GLOBECOM'12*, 2012.

[29] Y. Liu, Y. Shen, D. Guo, and M. Z. Win, "Network localization and synchronization using full-duplex radios," *IEEE Trans. Signal Process.*, vol. 66, no. 3, pp. 714–728, 2018.

[30] E. Everett, C. Shepard, L. Zhong, and A. Sabharwal, "Softnull: Many-antenna full-duplex wireless via digital beamforming," *IEEE Trans. Wireless Commun.*, vol. 15, no. 12, pp. 8077–8092, 2016.

[31] N. M. Gowda and A. Sabharwal, "JointNull: Combining partial analog cancellation with transmit beamforming for large-antenna full-duplex wireless systems," *IEEE Trans. Wireless Commun,*, vol. 17, no. 3, pp. 2094–2108, 2018.

[32] E. Aryafar and A. Keshavarz-Haddad, "PAFD: Phased array full-duplex," in *Proc. IEEE INFOCOM'18*, 2018.

[33] M. B. Dastjerdi, N. Reiskarimian, T. Chen, G. Zussman, and H. Krishnaswamy, "Full duplex circulator-receiver phased array employing self-interference cancellation via beamforming," in *Proc. IEEE RFIC'18*, 2018.

[34] G. C. Alexandropoulos, M. A. Islam, and B. Smida, "Full duplex hybrid A/D beamforming with reduced complexity multi-tap analog cancellation," in *Proc. IEEE SPAWC'20*, 2020.

[35] B. Sadhu, Y. Tousi, J. Hallin, S. Sahl, S. K. Reynolds, Ö. Renström, K. Sjögren, O. Haapalahti, N. Mazor, B. Bokinge *et al.*, "A 28-GHz 32-element TRX phased-array IC with concurrent dual-polarized operation and orthogonal phase and gain control for 5G communications," *IEEE J. Solid-State Circuits*, vol. 52, no. 12, pp. 3373–3391, 2017.

[36] D. P. Bertsekas and J. N. Tsitsiklis, "Convergence rate and termination of asynchronous iterative algorithms," in *Proc. ACM ICS'89*, 1989.

[37] D. Raychaudhuri, I. Seskar, G. Zussman, T. Korakis, D. Kilper, T. Chen, J. Kolodziejski, M. Sherman, Z. Kostic, X. Gu, H. Krishnaswamy, S. Maheshwari, P. Skrimponis, and C. Gutterman, "Challenge: COSMOS: A city-scale programmable testbed for experimentation with advanced wireless," in *Proc. ACM MobiCom'20*, 2020.

APPENDIX A
PROOF OF LEMMA 6.1

Since $\mathbf{w}^{(\kappa)}$ and $\mathbf{v}^{(\kappa)}$ are optimal solutions to (Opt-Tx) and (Opt-Rx) in the κ^{th} iteration, it holds that

$$\mathsf{Re}[\mathbf{s}_{\mathrm{t}}^{\top}\mathbf{w}^{(\kappa')}] = a_{\mathrm{t}}^{(\kappa')},\ \mathsf{Im}[\mathbf{s}_{\mathrm{t}}^{\top}\mathbf{w}^{(\kappa')}] = 0,\ (\kappa' = \kappa, \kappa+1)$$
$$\mathsf{Re}[\mathbf{s}_{\mathrm{r}}^{\top}\mathbf{v}^{(\kappa')}] = a_{\mathrm{r}}^{(\kappa')},\ \mathsf{Im}[\mathbf{s}_{\mathrm{r}}^{\top}\mathbf{v}^{(\kappa')}] = 0,\ (\kappa' = \kappa, \kappa+1),$$
$$(\mathbf{v}^{(\kappa)})^{\dagger}\mathbf{H}_{\mathbf{w}^{(\kappa)}}(f_k)\mathbf{v}^{(\kappa)} \cdot \tfrac{P_{\mathrm{t}}}{N} \le N\beta,\ \forall k,$$
$$(\mathbf{w}^{(\kappa+1)})^{\dagger}\mathbf{H}_{\mathbf{v}^{(\kappa)}}(f_k)\mathbf{w}^{(\kappa+1)} \cdot \tfrac{P_{\mathrm{t}}}{N} \le N\beta,\ \forall k.$$

Assume by contradiction that $F_{\mathrm{t}}^{(\kappa+1)}(a_{\mathrm{t}}^{(\kappa+1)}) < F_{\mathrm{t}}^{(\kappa+1)}(a_{\mathrm{t}}^{(\kappa)})$, we can select a new Tx beamformer $\widetilde{\mathbf{w}}^{(\kappa+1)} = \mathbf{w}^{(\kappa)}$ with an increased value of $F_{\mathrm{t}}^{(\kappa+1)}$ while satisfying all the constraints in (Opt-Tx). Similarly, $F_{\mathrm{r}}^{(\kappa+1)}(a_{\mathrm{r}}^{(\kappa+1)}) \ge F_{\mathrm{r}}^{(\kappa+1)}(a_{\mathrm{r}}^{(\kappa)})$ also holds. □

APPENDIX B
PROOF OF PROPOSITION 6.2

The proof is based on induction on κ and the structural properties of the objective functions (20). By taking the second derivatives of (20), it can be seen that

- $F_{\mathrm{t}}^{(\kappa+1)}(a_{\mathrm{t}})$ is symmetric w.r.t. $\psi_{\mathrm{t}}^{(\kappa+1)} = a_{\mathrm{r}}^{(\kappa)} + \frac{1}{2\alpha_{\kappa+1}}$ and is monotonically increasing for $a_{\mathrm{t}} \in (0, \psi_{\mathrm{t}}^{(\kappa+1)}]$ and monotonically decreasing for $a_{\mathrm{t}} \in (\psi_{\mathrm{t}}^{(\kappa+1)}, \infty)$,
- $F_{\mathrm{r}}^{(\kappa+1)}(a_{\mathrm{r}})$ is symmetric w.r.t.$\psi_{\mathrm{r}}^{(\kappa+1)} = a_{\mathrm{t}}^{(\kappa+1)} + \frac{1}{2\alpha_{\kappa+1}}$ and is monotonically increasing for $a_{\mathrm{r}} \in (0, \psi_{\mathrm{r}}^{(\kappa+1)}]$ and is monotonically decreasing for $a_{\mathrm{r}} \in (\psi_{\mathrm{r}}^{(\kappa+1)}, \infty)$.

The proof is based on the induction of κ.

Base Case ($\kappa = 0$): Let $\mathbf{w}^{(0)}$ and $\mathbf{v}^{(0)}$ be the initial Tx and Rx beamformers given by (21) with initial array factors:

$$a_{\mathrm{t}}^{(0)} = \mathbf{s}_{\mathrm{t}}^{\top}\mathbf{w}^{(0)} = \tfrac{1}{2} \cdot \beta^{1/4} N^{1/2} P_{\mathrm{t}}^{-1/4},$$
$$a_{\mathrm{r}}^{(0)} = \mathbf{s}_{\mathrm{r}}^{\top}\mathbf{v}^{(0)} = \tfrac{1}{2} \cdot \beta^{1/4} N^{1/2} P_{\mathrm{t}}^{-1/4}.$$

For $\kappa = 1$, $F_{\mathrm{t}}^{(1)}(a_{\mathrm{t}})$ is monotonically increasing for $a_{\mathrm{t}} \in (0, \psi_{\mathrm{t}}^{(1)}]$. Since $\frac{P_{\mathrm{t}}}{N} \ge N\beta$, it holds that

$$\psi_{\mathrm{t}}^{(1)} = a_{\mathrm{r}}^{(0)} + \tfrac{1}{2\alpha_1} = \tfrac{1}{2}(\beta^{1/4} N^{1/2} P_{\mathrm{t}}^{-1/4} + 1) \ge \beta^{1/4} N^{1/2} P_{\mathrm{t}}^{-1/4}.$$

One can then select $\mathbf{w}^{(1)} = 2\mathbf{w}^{(0)}$, which satisfies

$$a_{\mathrm{t}}^{(1)} = \mathbf{s}_{\mathrm{t}}^{\top}\mathbf{w}^{(1)} = \beta^{1/4} N^{1/2} P_{\mathrm{t}}^{-1/4}.$$

Since $|H_{mn}(f_k)| \le 1$ (see Section IV), it holds that

$$\begin{aligned}
&|(\mathbf{v}^{(0)})^{\top}\mathbf{H}(f_k)\mathbf{w}^{(1)}|^2 \cdot \tfrac{P_{\mathrm{t}}}{N} \\
&= \big|\textstyle\sum_{m=1}^{N}\sum_{n=1}^{N}(w_n H_{mn}(f_k) v_m)\big|^2 \cdot \tfrac{P_{\mathrm{t}}}{N} \\
&\le \big|\textstyle\sum_{m=1}^{N}\sum_{n=1}^{N}|w_n| \cdot |H_{mn}(f_k)| \cdot |v_m|\big|^2 \cdot \tfrac{P_{\mathrm{t}}}{N} \\
&\le \big|N^2 \cdot \tfrac{\beta^{1/4}}{N^{1/2}P_{\mathrm{t}}^{1/4}} \cdot \tfrac{\beta^{1/4}}{2N^{1/2}P_{\mathrm{t}}^{1/4}}\big|^2 \cdot \tfrac{P_{\mathrm{t}}}{N} = \tfrac{N\beta}{4} < N\beta.
\end{aligned}$$

Hence, there $\exists\ \mathbf{w}^{(1)}$ such that $a_{\mathrm{t}}^{(1)} > a_{\mathrm{t}}^{(0)}$ and all constraints in (Opt-Tx) are satisfied. Similarly, $a_{\mathrm{r}}^{(1)} > a_{\mathrm{r}}^{(0)}$ holds.

Inductive Step ($\kappa \ge 1$): Assuming that $a_{\mathrm{t}}^{(0)} \le \cdots \le a_{\mathrm{t}}^{(\kappa)}$ and $a_{\mathrm{r}}^{(0)} \le \cdots \le a_{\mathrm{r}}^{(\kappa)}$, we need to prove that $a_{\mathrm{t}}^{(\kappa)} \le a_{\mathrm{t}}^{(\kappa+1)}$ and $a_{\mathrm{r}}^{(\kappa)} \le a_{\mathrm{r}}^{(\kappa+1)}$. We consider two cases.

Case 1: $a_{\rm t}^{(\kappa)} \le a_{\rm r}^{(\kappa)}$. First, we show that $a_{\rm t}^{(\kappa+1)} \ge a_{\rm t}^{(\kappa)}$. Assume by contradiction that $a_{\rm t}^{(\kappa+1)} < a_{\rm t}^{(\kappa)} \le a_{\rm r}^{(\kappa)}$, and $a_{\rm t}^{(\kappa+1)}$ is achieved by $\mathbf{w}^{(\kappa+1)}$. Since $F_{\rm t}^{(\kappa+1)}(a_{\rm t})$ is monotonically increasing for $a_{\rm t} \in (0, \psi_{\rm t}^{(\kappa+1)}]$, it must hold that $F_{\rm t}^{(\kappa+1)}(a_{\rm t}^{(\kappa+1)}) < F_{\rm t}^{(\kappa+1)}(a_{\rm t}^{(\kappa)})$, contradicting Lemma 6.1.

Second, we show that $a_{\rm r}^{(\kappa+1)} \ge a_{\rm r}^{(\kappa)}$. Assume by contradiction that $a_{\rm r}^{(\kappa+1)} < a_{\rm r}^{(\kappa)}$. Recall that $F_{\rm r}^{(\kappa+1)}(a_{\rm r})$ has an axis of symmetry at $\psi_{\rm r}^{(\kappa+1)} = a_{\rm t}^{(\kappa+1)} + \frac{1}{2\alpha_{\kappa+1}}$, and is monotonically increasing for $a_{\rm r} \in (0, \psi_{\rm r}^{(\kappa+1)}]$. We consider the following cases based on the relationships between $a_{\rm r}^{(\kappa)}$, $a_{\rm t}^{(\kappa+1)}$, and $a_{\rm r}^{(\kappa+1)}$, as depicted in Fig. 15.

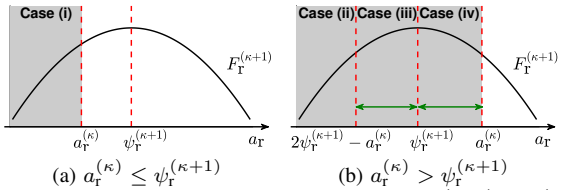

(a) $a_{\rm r}^{(\kappa)} \le \psi_{\rm r}^{(\kappa+1)}$ (b) $a_{\rm r}^{(\kappa)} > \psi_{\rm r}^{(\kappa+1)}$

Fig. 15: Illustration of Case 1 in the proof, where $\psi_{\rm r}^{(\kappa+1)} = a_{\rm t}^{(\kappa+1)} + \frac{1}{2\alpha_{\kappa+1}}$ and $a_{\rm r}^{(\kappa+1)} < a_{\rm r}^{(\kappa)}$ (shaded area) is assumed by contradiction.

Case (i): If $a_{\rm r}^{(\kappa)} \le \psi_{\rm r}^{(\kappa+1)}$ (see Fig 15(a)).

(i) Assume by contradiction that $a_{\rm r}^{(\kappa+1)} < a_{\rm r}^{(\kappa)} \le \psi_{\rm r}^{(\kappa+1)}$, it holds that $F_{\rm r}^{(\kappa+1)}(a_{\rm r}^{(\kappa+1)}) < F_{\rm r}^{(\kappa+1)}(a_{\rm r}^{(\kappa)})$, which contradicts Lemma 6.1.

Case (ii)–(iv): If $g_{\rm r}^{(\kappa)} > \psi_{\rm r}^{(\kappa+1)}$ (see Fig 15(b)).

(ii) If $a_{\rm r}^{(\kappa+1)} < 2\psi_{\rm r}^{(\kappa+1)} - a_{\rm r}^{(\kappa)} < \psi_{\rm r}^{(\kappa+1)} < a_{\rm r}^{(\kappa)}$, it is easy to see that one can select $\widetilde{\mathbf{v}}^{(\kappa+1)} = \mathbf{v}^{(\kappa)}$ that satisfies all the constraints and yields a higher value of the objective function $F_{\rm r}^{(\kappa+1)}(a_{\rm r})$.

(iii) If $2\psi_{\rm r}^{(\kappa+1)} - a_{\rm r}^{(\kappa)} \le a_{\rm r}^{(\kappa+1)} < \psi_{\rm r}^{(\kappa+1)} < a_{\rm r}^{(\kappa)}$, there exist a real number $\xi \in (0,1)$ such that $\xi a_{\rm r}^{(\kappa+1)} + (1-\xi) a_{\rm r}^{(\kappa)} = \psi_{\rm r}^{(\kappa+1)}$. Let $\widetilde{\mathbf{v}}^{(\kappa+1)} = \xi \mathbf{v}^{(\kappa+1)} + (1-\xi)\mathbf{v}^{(\kappa)}$. It holds that

$$
\begin{aligned}
&\widetilde{a}_{\rm r}^{(\kappa+1)} = \xi a_{\rm r}^{(\kappa+1)} + (1-\xi) a_{\rm r}^{(\kappa)} = \psi_{\rm r}^{(\kappa+1)},\\
&F_{\rm r}^{(\kappa+1)}(\widetilde{a}_{\rm r}^{(\kappa+1)}) > F_{\rm r}^{(\kappa+1)}(a_{\rm r}^{(\kappa+1)}),\\
&|\widetilde{v}_n^{(\kappa+1)}|^2 \le \xi^2 + (1-\xi)^2 + 2\xi(1-\xi) = 1,\\
&(\widetilde{\mathbf{v}}^{(\kappa+1)})^\dagger \mathbf{H}_{\mathbf{w}^{(\kappa+1)}}(f_k) \widetilde{\mathbf{v}}^{(\kappa+1)} \cdot \tfrac{P_{\rm t}}{N}\\
&\quad < \big[\xi \cdot (\mathbf{v}^{(\kappa+1)})^\dagger \mathbf{H}_{\mathbf{w}^{(\kappa+1)}}(f_k) \mathbf{v}^{(\kappa+1)}\\
&\qquad + (1-\xi) \cdot (\mathbf{v}^{(\kappa)})^\dagger \mathbf{H}_{\mathbf{w}^{(\kappa+1)}}(f_k) \mathbf{v}^{(\kappa)}\big] \cdot \tfrac{P_{\rm t}}{N} < N\beta,\ \forall k,
\end{aligned}
$$

where the last inequality comes from the fact that $\mathbf{H}_{\mathbf{w}^{(\kappa+1)}}(f_k)$ is Hermitian and positive semidefinite, and thus $(\mathbf{x}^\dagger \mathbf{H}_{\mathbf{w}^{(\kappa+1)}}(f_k)\mathbf{x})$ is convex with respect to $\mathbf{x}$.

(iv) If $\psi_{\rm r}^{(\kappa+1)} < a_{\rm r}^{(\kappa+1)} < a_{\rm r}^{(\kappa)}$, let $\widetilde{\mathbf{v}}^{(\kappa+1)} = \xi \mathbf{v}^{(\kappa+1)}$, where $\xi = \frac{\psi_{\rm r}^{(\kappa+1)}}{a_{\rm r}^{(\kappa+1)}} < 1$. Since $\widetilde{\mathbf{v}}^{(\kappa+1)}$ is linearly scaled down from $\mathbf{v}^{(\kappa+1)}$ by a factor of ξ, we have

$$
\begin{aligned}
&\widetilde{a}_{\rm r}^{(\kappa+1)} = \xi a_{\rm r}^{(\kappa+1)} < a_{\rm r}^{(\kappa+1)}, F_{\rm r}^{(\kappa+1)}(\widetilde{a}_{\rm r}^{(\kappa+1)}) > F_{\rm r}^{(\kappa+1)}(a_{\rm r}^{(\kappa+1)}),\\
&|\widetilde{v}_n^{(\kappa+1)}|^2 = \xi^2 \cdot |v_n^{(\kappa+1)}|^2 < 1,\ \forall n,\\
&(\widetilde{\mathbf{v}}^{(\kappa+1)})^\dagger \mathbf{H}_{\mathbf{w}^{(\kappa+1)}}(f_k) \widetilde{\mathbf{v}}^{(\kappa+1)} \cdot \tfrac{P_{\rm t}}{N}\\
&\quad = \xi^2 \cdot (\mathbf{v}^{(\kappa+1)})^\dagger \mathbf{H}_{\mathbf{w}^{(\kappa+1)}}(f_k) \mathbf{v}^{(\kappa+1)} \cdot \tfrac{P_{\rm t}}{N} < N\beta,\ \forall k.
\end{aligned}
$$

This contradicts the fact that $\mathbf{v}^{(\kappa+1)}$ is the optimal solution since $\widetilde{\mathbf{v}}^{(\kappa+1)}$ yields $F_{\rm r}^{(\kappa+1)}(\widetilde{a}_{\rm r}^{(\kappa+1)}) > F_{\rm r}^{(\kappa+1)}(a_{\rm r}^{(\kappa+1)})$ while satisfying constraints in (Opt-Rx).

Now the only marginal case left is $a_{\rm r}^{(\kappa+1)} = \psi_{\rm r}^{(\kappa+1)}$. Note that $a_{\rm t}^{(\kappa)} \le a_{\rm t}^{(\kappa+1)}$, and $a_{\rm r}^{(\kappa+1)} = \psi_{\rm r}^{(\kappa+1)} = a_{\rm t}^{(\kappa+1)} + \frac{1}{2\alpha_{\kappa+1}} < a_{\rm r}^{(\kappa)}$. Since $a_{\rm t}^{(\kappa+1)} \ge a_{\rm t}^{(\kappa)}$ and $\alpha_{\kappa+1} \le \alpha_\kappa$, we have $\psi_{\rm r}^{(\kappa+1)} \ge \psi_{\rm r}^{(\kappa)}$. Therefore, one can select $\widetilde{\mathbf{v}}^{(\kappa)} = \frac{a_{\rm r}^{(\kappa+1)}}{a_{\rm r}^{(\kappa)}} \cdot \mathbf{v}^{(\kappa)}$, which yields a higher value of the objective function $F_{\rm r}^{(\kappa)}(a_{\rm r})$ since it is decreasing for $a_{\rm r} \in [a_{\rm r}^{(\kappa+1)}, a_{\rm r}^{(\kappa)})$. This contradicts the fact that $\mathbf{v}^{(\kappa)}$ is optimal in the $\kappa^{\rm th}$ iteration and the proof of **Case 1** completes.

Case 2: $a_{\rm t}^{(\kappa)} > a_{\rm r}^{(\kappa)}$. The proof is similar to **Case 1** and thus is omitted here. □

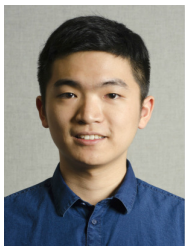

Tingjun Chen received the Ph.D. degree in electrical engineering from Columbia University in 2020, and the B.Eng. degree in electronic engineering from Tsinghua University in 2014. He is currently a Postdoctoral Associate at Yale University and will start as an Assistant Professor in the Department of Electrical and Computer Engineering at Duke University in Fall 2021. His research interests are in the areas of networking and communications with a specific focus on next-generation wireless networks and Internet-of-Things systems. He received the Google Research Scholar Award, the Facebook Fellowship, the Wei Family Private Foundation Fellowship, the Columbia Electrical Engineering Armstrong Memorial Award, and the ACM CoNEXT'16 Best Paper Award.

Mahmood Baraani Dastjerdi received the Ph.D. degree in electrical engineering from Columbia University in 2020, and the M.S. degree from Sharif University of Technology in 2014. His career is focused on the theory, design and experimental validation of analog/RF/millimeter-wave integrated circuits and systems. He joined MixComm Inc. as a member of technical staff in 2019. He is a recipient of the 2020 Columbia University Electrical Engineering Department Jury Award, the 2019 IEEE SSCS Predoctoral Achievement Award, the 2018 ADI ISSCC Outstanding Student Designer Award, and the Creative Tech Award in Engineering at the NYC Media Lab'18.

Harish Krishnaswamy received the Ph.D. degree in electrical engineering from USC in 2009. He is now an Associate Professor of Electrical Engineering at Columbia University and is the co-founder and CTO of MixComm Inc. His research interests span integrated devices, circuits, and systems for RF/mmWave/sub-mmWave applications. He received the Best Thesis in Experimental Research Award from the USC Viterbi School of Engineering, a DARPA Young Faculty Award, an IBM Faculty Award, an MTT-S Outstanding Young Engineer Award, several best paper awards including the IEEE ISSCC'07 Lewis Winner Award for Outstanding Paper, the 2015, 2018, 2020 IEEE RFIC Symposium Best Student Paper Awards, the 2020 IEEE IMS Best Student Paper Award, and the 2021 IEEE MTT-S Microwave Magazine Best Paper Award.

Gil Zussman received the Ph.D. degree in electrical engineering from the Technion in 2004 and was a postdoctoral associate at MIT in 2004–2007. He has been with Columbia University since 2007, where he is a Professor of Electrical Engineering and Computer Science (affiliated faculty). His research interests are in the area of networking, and in particular in the areas of wireless, mobile, and resilient networks. He is a co-recipient of 7 paper awards including the ACM SIGMETRICS'06 Best Paper Award, the 2011 IEEE Communications Society Award for Advances in Communication, and the ACM CoNEXT'16 Best Paper Award. He received the Fulbright Fellowship, the DTRA Young Investigator Award, two Marie Curie International Fellowships, and the NSF CAREER Award.